Charged hadron distributions in central and peripheral Si+A collisions at 14.6A GeV/c

T. Abbott,[4,a] Y. Akiba,[7] D. Beavis,[2] M. A. Bloomer,[9,b] P. D. Bond,[2] C. Chasman,[2] Z. Chen,[2] Y. Y. Chu,[2] B. A. Cole,[9,c] J. B. Costales,[9,d] H. J. Crawford,[3] J. B. Cumming,[2] R. Debbe,[2] J. Engelage,[3] S.-Y. Fung,[4] M. Gonin,[2] S. Gushue,[2] H. Hamagaki,[7] O. Hansen,[2,e] R. Hayano,[10] S. Hayashi,[2,7] S. Homma,[7] H. Z. Huang,[9,f] Y. Ikeda,[7,g] I. Juricic,[5,h] J. Kang,[4] S. Katcoff,[2] S. Kaufman,[1] K. Kimura,[8,i] K. Kitamura,[6,j] K. Kurita,[5,k] R. J. Ledoux,[9,d] M. J. Levine,[2] Y. Miake,[2,k] R. J. Morse,[9,b] B. Moskowitz,[2] S. Nagamiya,[5] J. Olness,[2] C. G. Parsons,[9,l] L. P. Remsberg,[2] H. Sakurai,[10] M. Sarabura,[9,m] P. Stankus,[5] S. G. Steadman,[9] G. S. F. Stephans,[9] T. Sugitate,[6] M. J. Tannenbaum,[2] Y. Tanaka,[8] J. H. Van Dijk,[2] F. Videbæk,[2] M. Vient,[4,n] P. Vincent,[2,o] V. Vutsadakis,[9] H. E. Wegner,[2] D. S. Woodruff,[9] Y. D. Wu,[5] and W. A. Zajc[5]

(E-802 Collaboration)

[1] *Physics Division, Argonne National Laboratory, Argonne, Illinois 60439*

[2] *Alternating Gradient Synchrotron, Chemistry and Physics Departments, Brookhaven National Laboratory, Upton, New York, 11973*

[3] *Space Sciences Laboratory, University of California, Berkeley, California 94720*

[4] *University of California, Riverside, California 92507*

[5] *Columbia University, New York, New York 10027 and Nevis Laboratories, Irvington, New York 10533*

[6] *Department of Physics, Hiroshima University, Hiroshima 730, Japan*

[7] *Institute for Nuclear Study, University of Tokyo, Tanashi, Tokyo 188, Japan*

[8] *Kyushu University, Fukuoka 812, Japan*

[9] *Massachusetts Institute of Technology, Cambridge, Massachusetts 02139*

[10] *Department of Physics, University of Tokyo, Tokyo 113, Japan*

(Received 30 March 1994)

The AGS spectrometer experiment E-802 has measured transverse mass spectra for charged hadrons over a wide rapidity interval in Si+Au, Si+Cu, and Si+Al reactions at 14.6A GeV/c. These results are compared for two different trigger conditions: central collisions corresponding to 7% of the inelastic cross section selected on multiplicity of charged particles and peripheral collisions corresponding to roughly 50% of the inelastic cross section selected on high kinetic energy at zero degrees. The invariant spectra are well described by exponentials in transverse mass allowing the extraction of rapidity distributions and inverse slope parameters for each specie emitted in the different reactions.

PACS number(s): 13.85.Ni, 25.75.+r

I. INTRODUCTION

The ultrarelativistic heavy ion programs initiated about 8 years ago both at Brookhaven (BNL) and CERN reveal properties of nuclear matter under extreme conditions. The concept of a quark-gluon plasma predicted for heavy ion collisions [1] has been a driving force for the experimental studies of nuclei at high energy density and high baryon density. A primary goal has been to quantify the amount of energy that is deposited in the target nucleus. Another important issue has been to determine whether or not nucleus-nucleus collisions can be described as a superposition of independent nucleon-nucleon collisions. To these ends a systematic measurement of Si-induced reactions on Al, Cu, and Au targets has been performed by the E-802 collaboration at the BNL Tandem-AGS accelerator complex with a beam momentum of 14.6A GeV/c. The rapidity distributions of the different charged hadrons emitted in the collisions as well as their momentum spectra provide the main information. Comparison of central and peripheral collisions for different target masses sheds light on the space-time evolution of particle production and rescattering in hadronic matter.

The organization of the paper is as follows. Section II describes the experimental details and the data analysis. Section III presents the data for the three targets for both peripheral collisions and central collisions. In Sec. IV the

[a]Now at Reedley College, Reedley, CA 93654.

[b]Now at Lawrence Berkeley Laboratory, Berkeley, CA 94720.

[c]Now at Columbia University, New York, NY 10027 and Nevis Laboratories, Irvington, NY 10533.

[d]Now at Radionics Software Applications Corp., Brookline, MA 02146.

[e]Now at Niels Bohr Institute for Astronomy, Physics, and Geophysics, DK-2100 Copenhagen Ø, Denmark.

[f]Now at Purdue University, West Lafayette, IN 47907.

[g]Now at Hitachi Limited, Hitachi, Ibaraki 316, Japan.

[h]Now at Schlumberger Corp., Houston, TX 77210.

[i]Now at Nagasaki Institute of Applied Science, Nagasaki 851-01, Japan.

[j]Now at NTT, Tsuyama, Tsuyama, Okayama 708, Japan.

[k]Now at University of Tsukuba, Tsukuba, Ibaraki 305, Japan.

[l]Now at NITON, Bedford, MA 01730.

[m]Now at 24B Bigelow St., Cambridge, MA 02139.

[n]Now at UC at Irvine, Irvine, CA 92717.

[o]Now at Bruker Inc., Karlsruhe, Germany.

data are compared to previous data published by E-802 and to data published by other AGS experiments. Energy and momentum conservation are evaluated in Sec. V. Discussions and a summary are contained in Sec. VI.

II. EXPERIMENTAL DETAILS AND DATA ANALYSIS

The experimental setup is briefly described below while a full description of the E-802 experimental setup can be found in Ref. [2]. Descriptions of the previous data analysis of E-802 have been presented in Refs. [3–5].

A. Experimental details

The data were obtained in December 1988 and June 1989 using the E-802 spectrometer, the intensity of the ^{28}Si beam was typically 1×10^5 particles/spill in 1988 and 4×10^4 particles/spill in 1989 (with each spill $\simeq$600 ms long and $\simeq$4 s apart) and the beam size on the target was typically $\simeq$ 4 mm horizontally and $\simeq$ 2 mm vertically. The thickness of the Al and Cu targets were 3% of an interaction length (817 mg/cm^2 and 1440 mg/cm^2, respectively) and the thickness of the Au target was 3% of an interaction length (2939 mg/cm^2) for the December 1988 run and 1% (944 mg/cm^2) for the June 1989 run. Target-out runs were performed to determine background contributions. In general, target-out contributions to the spectra are very small and mainly affect the cross-section normalization.

The experimental arrangement consists of a rotatable 25 msr magnetic spectrometer ($5° \leq \theta \leq 58°$) with particle identification along with global event characterization detectors for the charged-particle multiplicity (TMA), a zero degree calorimeter which measures the kinetic energy of the projectile spectators (ZCAL), and a segmented lead-glass calorimeter (PbGl) for neutral transverse energy. The charged-particle multiplicity detector (TMA) surrounds the target with almost full azimuthal coverage. It consists of two sections: one section (barrel) covers polar angles from 31° to 149° while another section (wall) covers polar angles from 6° to 40°. The TMA has an opening on the side for the spectrometer and counts protons with scattered momentum, $p \geq 300$ MeV/c, and charged pions with momentum, $p \geq 50$ MeV/c. ZCAL [6] has an area of 60×60 cm^2 and is located downstream of the target with its face subtending an angle of ±1.5° at the target. Drift chambers are used for particle tracking, and a time-of-flight (TOF) wall supplemented by an optically segmented gas Cerenkov detector (GASC) provides the particle identification. The drift chambers are placed before ($T1, T2$) and after ($T3, T4$) the dipole magnet; the one-track resolution of the drift chambers is $\simeq$ 150 μm while two-track resolution is $\simeq$2 mm. TOF consists of 160 plastic scintillators (1.6 cm×1.6 cm×78 cm each) placed 6.5 meters from the target with a timing resolution of $\sigma \simeq$80 ps. The gas Cerenkov detector consists of a single volume of 4 atm Freon-12 with 40 segmented cells (23 cm×28 cm each) placed behind

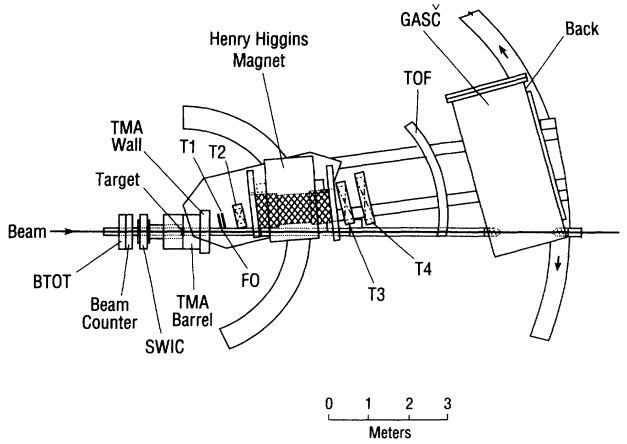

FIG. 1. E-802 spectrometer at $\theta_{\rm spec} = 5°$. The magnetic-field volume is represented as the cross-hatched area. SWIC is part of the beam diagnostic detectors. See text for further description of the detector elements.

the time-of-flight wall; the confirmation of particles after TOF and GASC is done with a wall (BACK) of two layers of plastic streamer tubes (24×64 elements) placed just behind GASC. A set of 21 plastic scintillator counter ($F0$) is placed in front of $T1$ for trigger purposes. A layout of the E-802 spectrometer at $\theta_{\rm spec} = 5°$ is presented in Fig. 1.

A set of plastic scintillator counters placed upstream of the target defines the "good" beam while rejecting pileup and beam halo. The correct geometry of the beam is first defined by four scintillator counters (up, down, east, and west) placed $\simeq$ 3 meters upstream of the target (UDEW). Good beam is selected by requiring the correct charge ($Z = 14 \pm 1.6$) and by rejecting pile-up, from scintillators (BTOT, BTOF) placed closer to the target. These detectors also provide the timing for the trigger logic and time-of-flight measurements ($\sigma \simeq$ 40 ps). Finally, a scintillator with a 1-cm-diameter hole situated 1 meter before the target rejects beam halo (BVETO). A plastic scintillator "bull's eye" counter (BE) downstream of the target (10.5 meters) in front of the zero degree calorimeter is used to reject events with beam remnants near Z=14.

B. Spectrometer acceptance

The acceptance for the E-802 spectrometer imposed by geometry and particle identification limits is shown versus rapidity and transverse momentum (y, p_t) for pions, kaons, protons, and deuterons in Figs. 2(a) and 2(b). These acceptances result from five different spectrometer angle settings, $\theta_{\rm spec} = 5°$, 14°, 24° 34°, and 44°, where $\theta_{\rm spec}$ is the smallest angle covered by the spectrometer and different magnetic field settings. For each angle setting, the spectrometer covers a polar angle range of ($\theta_{\rm spec} \leq \theta \leq \theta_{\rm spec} + 14°$). The rapidity gap between a target and projectile nucleon is 3.44 for a beam momentum of 14.6A GeV/c and the rapidity acceptance of the spectrometer is roughly centered near midrapidity for pi-

ons, while for heavier particles, the rapidity acceptance is shifted to lower values. The spectrometer covers approximately a rapidity range of $0.4 \leq y \leq 2.2$ for protons, $0.4 \leq y \leq 1.6$ for deuterons, $0.6 \leq y \leq 2.8$ for pions, and $0.6 \leq y \leq 2.0$ for kaons. The particle identification of the spectrometer extends up to a momentum, p, of $\simeq 5.2$ GeV/c for pions, $p \simeq 3.6$ GeV/c for kaons, $p \simeq 10$ GeV/c for protons, and $p \simeq 6$ GeV/c for deuterons. For particle identification, symmetric cuts $\pm 3\sigma$ have been applied in the $(p, 1/\beta)$ plane, where p is the momentum of the particle and β its velocity. The gas Cerenkov counter has been used to reject electrons from pions in the momentum range $0.6 < p < 1.4$ GeV/c and kaons from pions in the momentum range 2.2 GeV/$c \leq p \leq 5.2$ GeV/c.

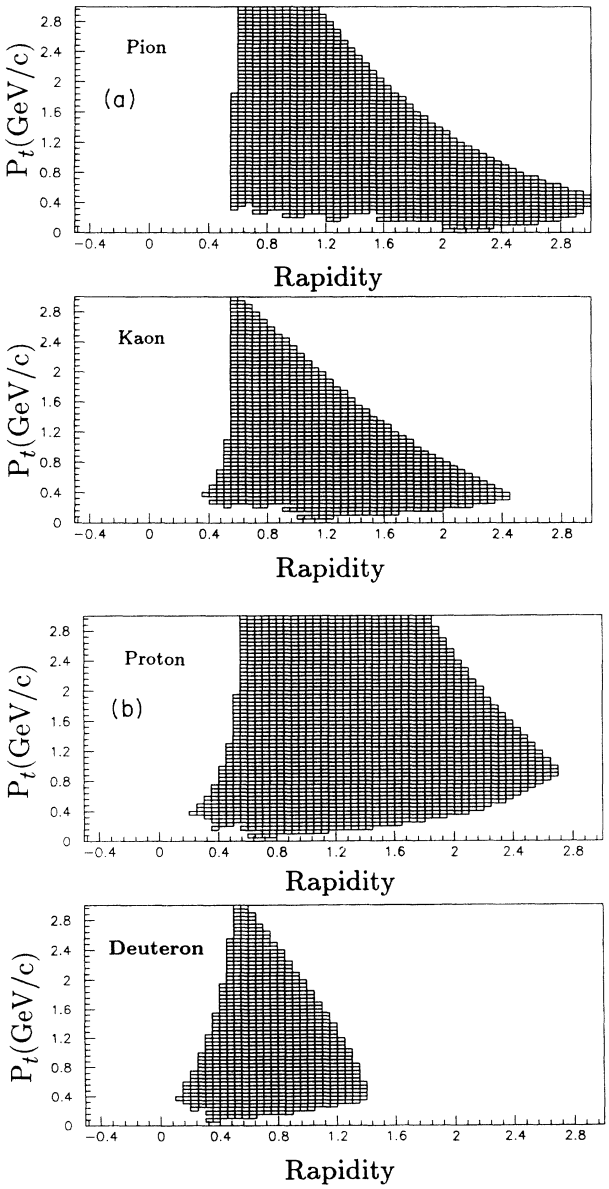

FIG. 2. (a) E-802 acceptance in rapidity and transverse momentum for pions and kaons. The bin size (Δy=0.05, Δp_t=50 MeV) corresponds to the bin size used in the analysis. (b) E-802 acceptance in rapidity and transverse momentum for protons and deuterons.

The gas Cerenkov counter also provided the rejection of pions from protons in the momentum range of 2.2 GeV/$c \leq p \leq 10$ GeV/c and rejection of kaons from protons in the momentum range of 5.2 GeV/$c \leq p \leq 10$ GeV/c. Due to the timing resolution of the time-of-flight counter, kaon contamination in identified protons reaches $\simeq$5% for the momentum interval 3.6 GeV/$c \leq p \leq 5.2$ GeV/c. For momenta $p \geq 6.0$ GeV/c the fraction of deuterons misidentified as protons does not exceed $\simeq$6% of the total protons. These effects are included in the systematic error estimate for the proton data. To distinguish deuterons from alphas (a very small contamination), charge cuts on the energy loss recorded in the time-of-flight counter have been done.

C. Hardware triggers

The normalizations required for data analysis were achieved with data using a minimum bias trigger, INT. This trigger is satisfied when the charge detected in the downstream scintillator counter (BE) is less than the silicon beam charge by at least 1.3 units. The measured interaction cross sections are $\sigma_{\rm INT} = 3.75 \pm 0.19$ barns for Si+Au, $\sigma_{\rm INT} = 2.17 \pm 0.11$ barns for Si+Cu and $\sigma_{\rm INT} = 1.45 \pm 0.09$ barns for Si+Al. The quoted errors are systematic and result from the correction for target-out contributions. These values are in excellent agreement with the measurements from the PbGl detector [7]. Two other first level triggers, SPEC and TMA, were implemented in hardware for data acquisition. SPEC is satisfied when hits are recorded both in front of the spectrometer magnet (in $F0$) and in the time-of-flight (TOF) wall. Central collisions are identified with TMA by requiring that the total charged multiplicity recorded in the Target Multiplicity Array corresponds to roughly the upper 7% of the total distribution. Different scale-down factors were used to modify the trigger mixing as a function of the spectrometer angle. All triggers required a valid beam trigger (BEAM). The different triggers can be represented logically as

$$BEAM = \overline{PRE} \cap \overline{UDEW} \cap BTOT \cap BTOF \cap \overline{BVETO} ,$$

$$INT = BEAM \cap \overline{BE} ,$$

$$SPEC = BEAM \cap TOF \cap F0 ,$$

$$TMA = BEAM \cap TMA ,$$

where PRE is a 300-ns pile-up rejection criterion.

D. Software cuts

For "central" collisions, TMA and SPEC hardware triggers were used to analyze the data for the Au target. Due to significant background (empty target) in the TMA distributions for the light targets, only the SPEC trigger was used for the Al and Cu targets. Such background events have negligible influence on the Au target results due to their low multiplicity. In addition, central collisions were selected by using software cuts on the total charged particle multiplicities as recorded by the target multiplicity array, allowing only events with multiplicities above a sharp threshold. These thresholds were chosen such that the trigger cross sections were 7% of the inter-

action cross sections given above. Figure 3 illustrates the cut $M_{\rm ch} \geq 175$ on the charge multiplicity for central collisions in the Si+Au reaction with a 3% target. This cut decreases to $M_{\rm ch} \geq 154$ using the 1% interaction length Au target due to reduced gamma conversion and smaller production of delta electrons in the thinner target. The spectrum shown in the figure is generated with the INT trigger with no correction for target-out events. However, because of the lower cut for Si+Cu ($M_{\rm ch} \geq 97$) and Si+Al ($M_{\rm ch} \geq 62$), significant corrections were made due to the target-out contributions. For a given target, the value of the multiplicity threshold was constant to within 3% over the entire running period.

To analyze "peripheral" collision events, SPEC hardware trigger was used for the three targets. In addition, a software cut on the kinetic energy spectra of the projectile spectators measured by ZCAL, $T_{\rm ZCAL} \geq 250$ GeV ($T_{\rm beam}$=383 GeV), was used to define peripheral collisions as $\simeq$ 50% of the interaction cross section. This cut corresponds to 45% of the interaction cross section for the Si+Au reaction, 50% for Si+Cu, and 58% for Si+Al. Figure 4 shows a distribution of $T_{\rm ZCAL}$ for minimum bias events in Si+Cu, including the target-out contributions. The limit of 250 GeV was used for $\theta_{\rm spec} \geq 14°$. Because the spectrometer partially obscures the zero degree calorimeter at $\theta_{\rm spec} = 5°$ (see Ref. [2]), the cut was modified to $T_{\rm ZCAL} \geq 215$ GeV at this spectrometer setting to obtain approximately the same cross sections and multiplicity distributions. For central events, the zero degree calorimeter was also used as a trigger for Si+Al (7% cut, $T_{\rm ZCAL} \leq 80$ GeV) to compare with the results obtained with the target multiplicity array since the zero degree calorimeter has practically no target-out contribution. The two data sets for central Si+Al are in good agreement within systematic errors.

For each software cut using TMA triggers, the trigger cross section $\sigma_{\rm trig}$ was defined as

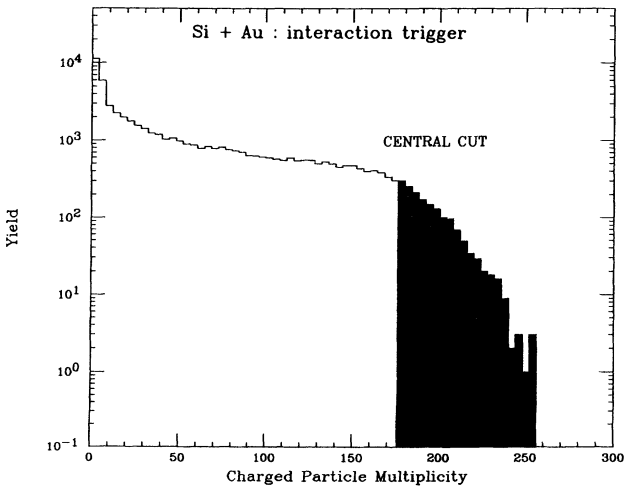

FIG. 3. Charged multiplicity for minimum bias collisions in the Si+Au reaction. The threshold corresponding to 7% of the interaction cross section is shown. Target-out contributions have not been subtracted.

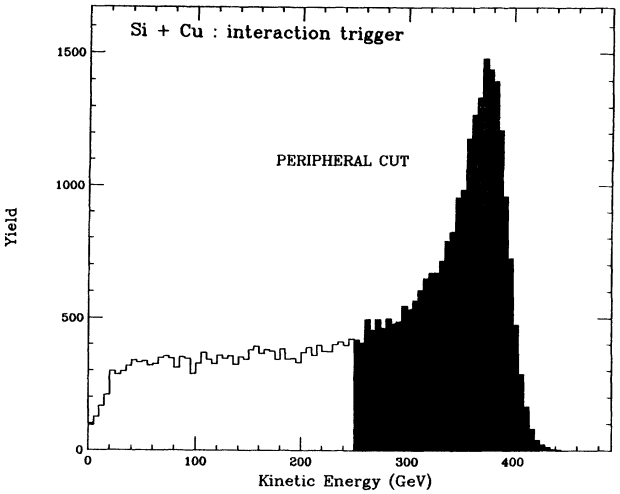

FIG. 4. Kinetic energy spectra of the projectile spectators in the Si+Cu reaction. The threshold corresponding to roughly 50% on the interaction cross section is shown. Target-out contributions have not been subtracted.

$$\sigma_{\rm trig} = \left(\frac{N_{\rm trig}}{N_{\rm beam}} - \frac{N_{\rm trig}^{\rm background}}{N_{\rm beam}^{\rm background}} \right) * C \ ({\rm mb}) \ , \qquad (1)$$

where C is a constant depending on the target thickness. $N_{\rm trig}$ is the number of events for a given software cut and $N_{\rm trig}^{\rm background}$ is the corresponding number for target out events. $N_{\rm beam}$ is the number of incident particles and $N_{\rm beam}^{\rm background}$ is the number of incident particles in the background study. For SPEC triggers, the trigger cross section $\sigma_{\rm trig}$ was obtained with (1) using INT trigger events. For central collisions, as already mentioned, the trigger cross section was $\sigma_{\rm trig}$=0.07 $\sigma_{\rm INT}$ for the three targets. For peripheral collisions, $\sigma_{\rm trig}$=0.58 $\sigma_{\rm INT}$ for Si+Al, $\sigma_{\rm trig}$=0.50 $\sigma_{\rm INT}$ for Si+Cu, and $\sigma_{\rm trig}$=0.45 $\sigma_{\rm INT}$ for Si+Au.

E. Efficiencies and corrections

The yield of pions and kaons was corrected to account for decay in flight. The kaon correction is given by the factor $\exp(d/\beta\gamma c\tau)$ where τ is the mean life, βc the velocity, and d the path length from the target to the time-of-light counter. However, the correction for pions cannot be done using this simple approach, since a large fraction of the decay muons have a sufficiently small deflection that their track will be still reconstructed and identified as a pion. The pion decay correction is estimated from Monte Carlo simulations taking into account the various cuts included in the tracking program [8]. This correction is $\simeq$ 1% at high momentum (2 GeV/c) and $\simeq$ 20% at low momentum (0.5 GeV/c).

Low momentum charged particles suffer significant multiple scattering when traversing the target, the beam pipe, and the spectrometer. It is expected that the magnitude of this effect increases, for a given momentum, with the mass of the emitted particle. Monte Carlo simu-

lations based on GEANT [9] routines have been performed to estimate particle loss for the E-802 spectrometer [10]. The results of the Monte Carlo were approximated by analytical functions as a function of momentum and were included in the acceptance calculations. The particle loss is significant for protons and deuterons and applied for momenta $p \leq 1$ GeV/c. For instance, the correction is $\simeq$ 10% at 0.7 GeV/c and 0.2 GeV/c momentum for protons and pions, respectively. Because of the multiple scattering corrections, the target cuts used to determine whether or not the emitted particles originate from the target were estimated based on Monte Carlo simulations. The cuts were ± 3 (cm) in x and y directions with the (x, y) plane is defined as a plane perpendicular to the beam direction (z axis) with its origin at the target center (z=0).

As a result of the rotation of the E-802 spectrometer the four tracking chambers appear to move relative to one another within elastic limits. Such positioning variations result in a change of the apparent target position. These shifts are taken into account in the present analysis. They also affect the determination of the absolute momentum of emitted particles and result in a change in the momentum determination of up to 3% with respect to previous E-802 data analyses.

The effect of dead slats in the time-of-flight wall was studied with Monte Carlo simulations [8]. The number of nonworking slats did not exceed 2–3 % of the total number of slats and corrections for this have been included in the total acceptance calculations.

The overall reconstruction efficiency for the analysis is estimated to be 83%. This number includes a tracking efficiency of 85% [11] and a particle identification efficiency of 98%. The latter inefficiency is due to cuts applied on the time-of-flight wall in the x (± 4 cm) and y (± 6 cm) directions. These cuts are needed to check the consistency between the tracking information and the time-of-flight hits and to reject background particles.

F. Invariant spectra

Multiplicities per unit of rapidity and transverse momentum, $d^2N/dp_t dy$, are shown in Figs. 5 and 6 for protons and pions emitted in Si+Au central collisions. As can be seen the measurement extends to $p_t \simeq 2$ GeV/c for protons and up to $p_t \simeq 1.5$ GeV/c for pions. For kaons (not shown) the maximum p_t value is $\simeq$ 1.2 GeV/c. The differential invariant multiplicity distribution is defined as

$$E(d^3N/dp^3) = (1/\sigma_{\rm trig})(1/2\pi m_t)(d^2\sigma/dm_t dy) \ , \qquad (2)$$

where m_t is the transverse mass

$$m_t = (p_t^2 + m^2)^{1/2} \ . \qquad (3)$$

Figures 7–12 show the resulting invariant spectra in units of GeV^{-2} (c=1) versus $m_t - m$ for each particle specie for the three targets and the two trigger conditions and each rapidity interval. The lowest spectrum

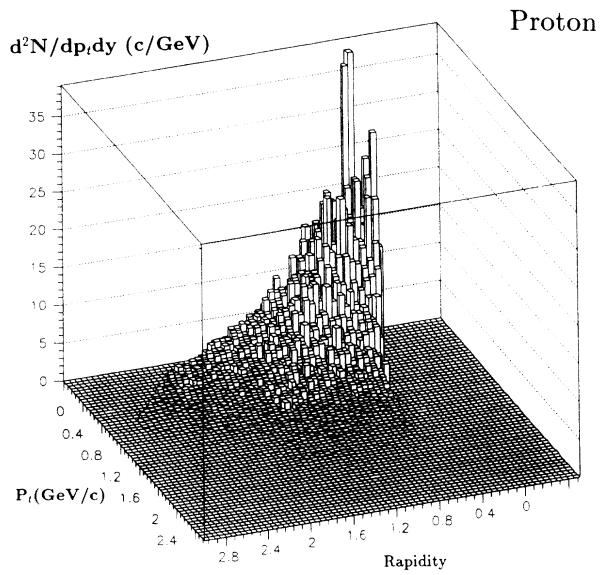

FIG. 5. Proton multiplicity per unit of rapidity and transverse momentum for central collisions in the Si+Au reaction.

corresponds to the highest rapidity value. For protons and pions the nth spectrum has been multiplied by 10^{-n} starting with n=0 at lowest rapidity. Because of poorer statistics for the deuterons and kaons, their nth spectra has been multiplied by 10^{-2n}. Note that wider rapidity bins were used for all K^- and some K^+ spectra.

Within the spectrometer acceptance and the statistical fluctuations, the invariant spectra for all particles seem to be described by an exponential function, as can be seen in Figs. 7–12. Consequently, an exponential function

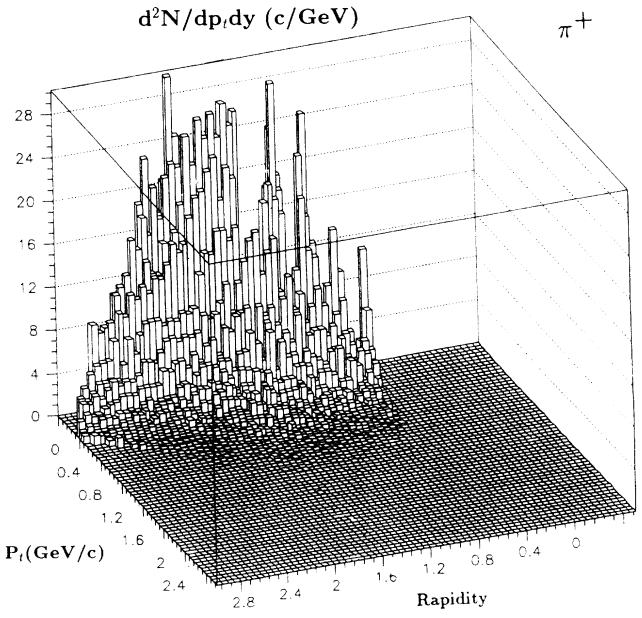

FIG. 6. π^+ multiplicity per unit of rapidity and transverse momentum for central collisions in the Si+Au reaction.

$Ae^{-(m_t-m)/T}$ where T is called the inverse slope parameter has been fit to each invariant spectrum. These fits, represented by solid lines in Figs. 7–12, were performed by the maximum likelihood procedure for Poisson statistics [12]. The overall distribution of χ^2 per degree of freedom is around 0.5–2. Higher values are obtained for π^- spectra in Si+Au central collisions at $y \simeq 2.5$ where some deviation from the exponential form at low (m_t-m) is observed. The errors in A and T are obtained from the diagonal terms (σ_A^2, σ_T^2) of the error matrix given by the fitting routines [12] which include the effect of correlations between the parameter A and the parameter T. These two parameters are not uncorrelated. Indeed, the overall distribution of the correlation coefficient defined by $\sigma_{AT}^2/(\sigma_A\sigma_T)$ is negative and in the range of 0.8–0.9.

The final multiplicity density, dN/dy, is obtained by integration, from $m_t - m$=0 to $m_t - m = \infty$, of the exponential function and can be written as

$$\frac{dN}{dy} = 2\pi AT(T+m) \ . \tag{4}$$

For negative pions, this extrapolation does not include the steeper component observed by the E-810 collaboration at high rapidities (see Sec. IV). The error (standard deviation) for dN/dy is evaluated from the deviation of the right term of the formula in Eq. (4) using the variances and covariance for A and T.

Values of dN/dy and T are listed in Tables I–VI as a function of the rapidity interval for the three targets and the two trigger conditions. Errors quoted in the table are statistical errors only.

G. Systematic errors on dN/dy and T

The uncertainties shown and quoted in this paper are statistical errors only except where specifically noted. Er-

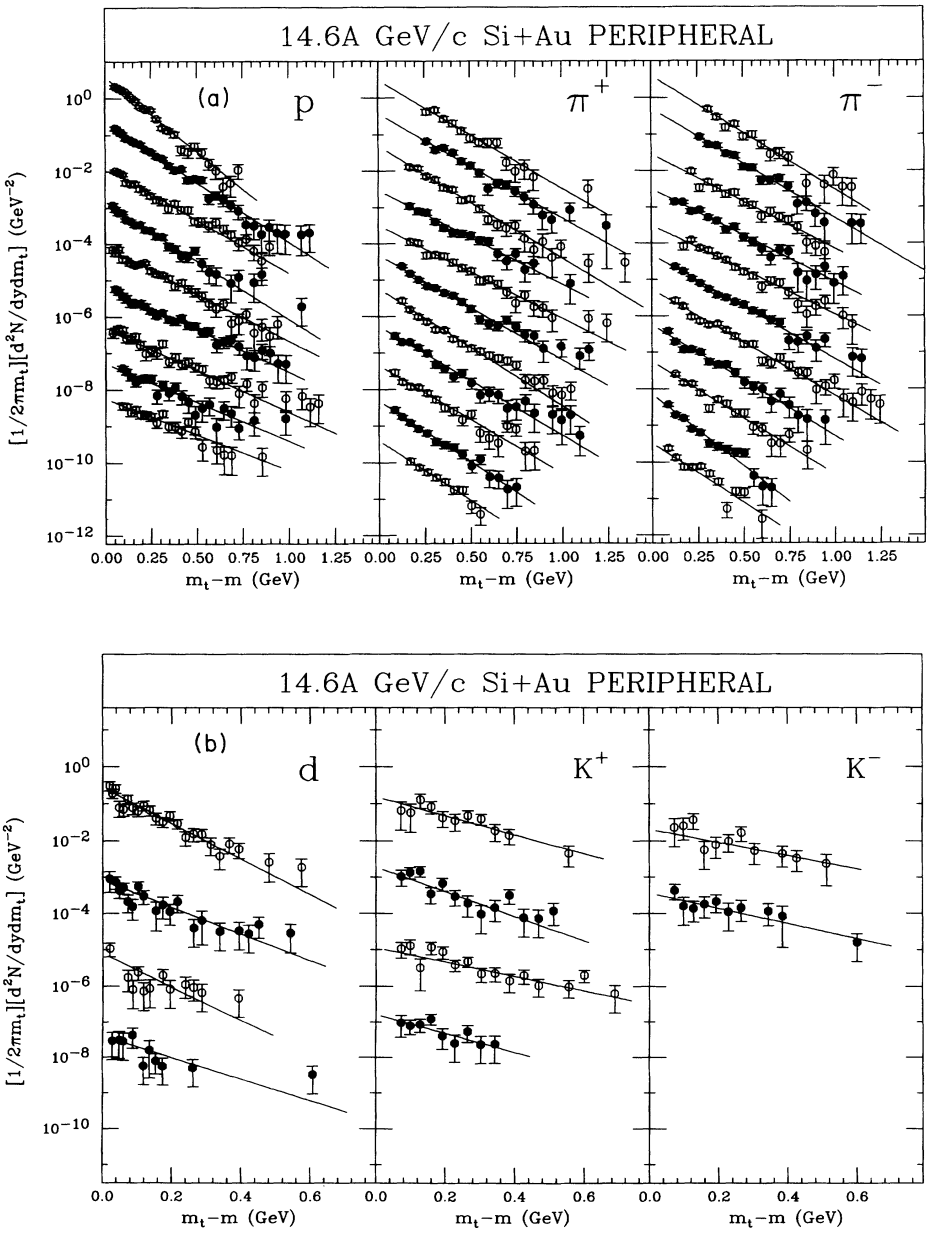

FIG. 7. (a) Invariant spectra for Si+Au peripheral collisions. For protons, the rapidity interval is y=0.50 (top spectrum) to y=2.1 (bottom spectrum) with Δy=0.20. For pions, the rapidity interval is y=0.70 (top spectrum) to y=2.7 (bottom spectrum) with Δy=0.20. Each successive spectrum is divided by 10. Only statistical errors are shown. Systematic errors are discussed in Sec. II G. (b) Same as (a). For deuterons, the rapidity interval is y=0.50 (top spectrum) to y=1.1 (bottom spectrum) with Δy=0.20. For K^+, the rapidity interval is y=0.90 (top spectrum) to y=2.1 (bottom spectrum) with Δy=0.40. For K^-, the rapidity interval is y=1.3 (top spectrum) to y=1.9 (bottom spectrum) with Δy=0.60. Each successive spectrum is divided by 100. Only statistical errors are shown. Systematic errors are discussed in Sec. II G.

rors smaller than the size of the symbol points are not shown. The systematic error for the dN/dy results is estimated to be $\pm(10\text{–}15)\%$. This comes from errors in tracking efficiency ($\pm 8\%$), consistency check between different spectrometer settings ($\pm 4\%$), acceptance calculations ($\pm 5\%$), and particle identification ($\pm 2\%$). These errors are assumed to be incoherent. Tracking efficiency was obtained by comparing the results of visual scanning of several hundred events using the E-802 event display with the output of the tracking program [11]. These events were taken with the spectrometer at 14°. Errors in tracking efficiency result from scanning multiplicity bias and from extrapolation of the tracking efficiency obtained at 14° to other spectrometer settings. The overlap region of acceptance between two spectrometer settings ($\theta_{\text{spec}} = 14°$ and $\theta_{\text{spec}} = 5°$, for instance) provides an internal consistency check for the quality of the data. The number of counts in the overlap regions $(\Delta\theta, \Delta p_t)$ has been compared for π^+ and π^- and was found to agree within $\pm 10\%$. Estimates of the errors in the acceptance calculations were obtained by changing the size of the effective area of the detectors and the apparent target position in the x and y directions. The errors for particle identification are estimated from variations made in the software cuts.

The systematic error on the inverse slope parameter T is $\simeq \pm 10\%$. This is due largely to variations from the rapidity binning and normalization between different spectrometer settings. For the protons, the systematic error for T reaches 15% because of the K^+ and deuteron contaminations. It should be emphasized that the value of the inverse slope parameter T may in addition depend on the range $(m_t - m)$ used in the fitting procedure. This effect is not included in the systematic error estimates.

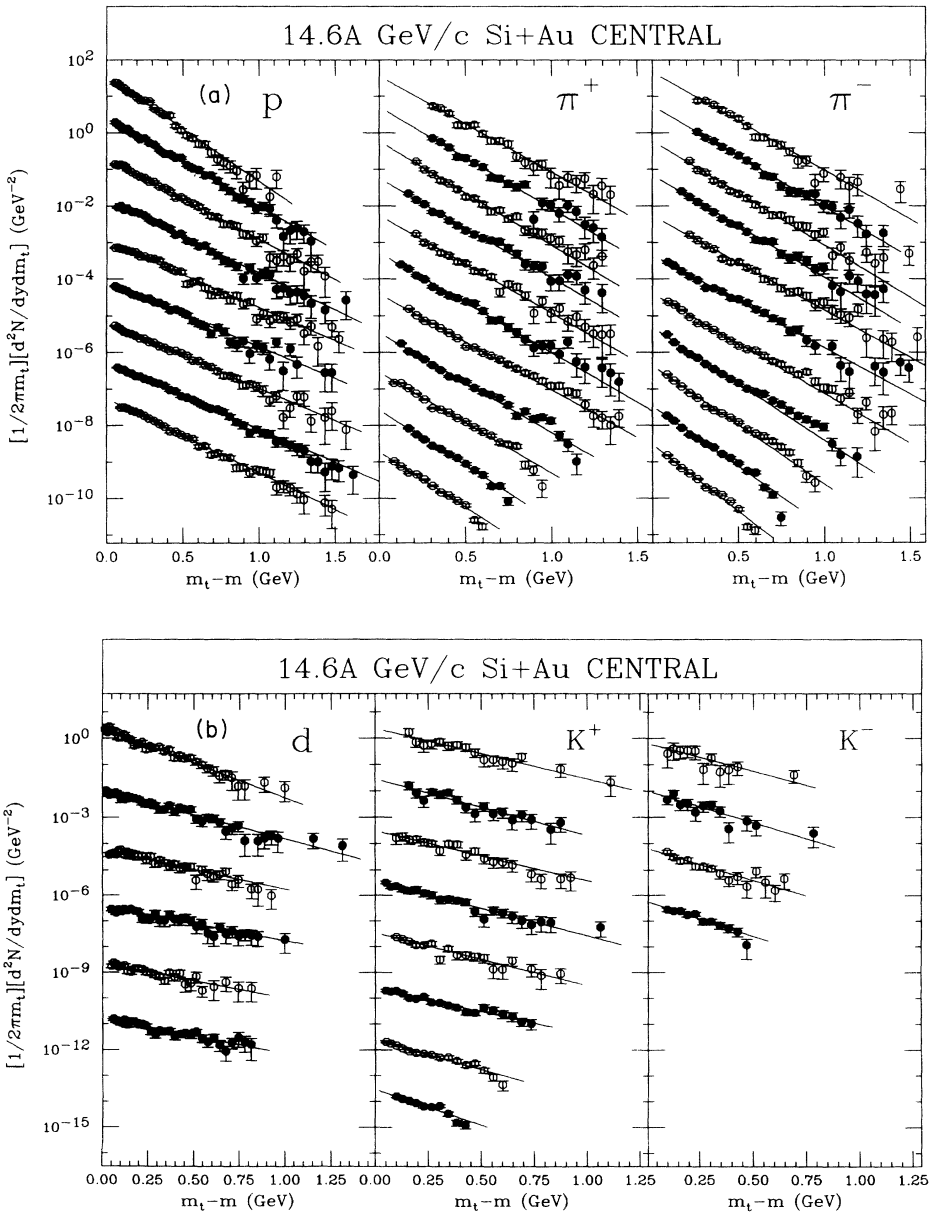

FIG. 8. (a) Invariant spectra for Si+Au central collisions. For protons, the rapidity interval is y=0.50 (top spectrum) to y=2.1 (bottom spectrum) with Δy=0.20. For pions, the rapidity interval is y=0.70 (top spectrum) to y=2.7 (bottom spectrum) with Δy=0.20. Each successive spectrum is divided by 10. Only statistical errors are shown. Systematic errors are discussed in Sec. II G. (b) Same as (a). For deuterons, the rapidity interval is y=0.50 (top spectrum) to y=1.5 (bottom spectrum) with Δy=0.20. For K^+, the rapidity interval is y=0.70 (top spectrum) to y=2.1 (bottom spectrum) with $\Delta y = 0.20$. For K^-, the rapidity interval is $y = 0.90$ (top spectrum) to $y = 2.1$ (bottom spectrum) with Δy=0.40. Each successive spectrum is divided by 100. Only statistical errors are shown. Systematic errors are discussed in Sec. II G.

TABLE I. Multiplicity density dN/dy as function of the rapidity interval. The data are listed for Si+Au central and peripheral collisions. Errors quoted are statistical errors. The systematic error is estimated to be ±(10–15)% (see Sec. II G).

PERIPHERAL COLLISIONS						
Rapidity	Proton	Deuteron	π^+	π^-	K^+	K^-
0.50	2.71±0.08	0.306±0.021				
0.70	1.96±0.06	0.118±0.013	0.984±0.090	0.984±0.085		
0.90	1.39±0.05	0.090±0.020	1.03±0.09	1.30±0.07	0.108±0.016	
1.10	1.23±0.04	0.072±0.030	1.19±0.07	0.922±0.086		
1.30	0.982±0.035		0.950±0.058	1.06±0.06	0.094±0.017	0.023±0.005
1.50	0.855±0.035		1.04±0.06	1.10±0.08		
1.70	0.749±0.038		1.32±0.04	1.35±0.05	0.112±0.013	
1.90	0.763±0.050		1.34±0.04	1.45±0.05		0.033±0.007
2.10	0.906±0.061		1.39±0.06	1.43±0.07	0.109±0.021	
2.30			1.17±0.05	1.38±0.07		
2.50			1.07±0.05	1.24±0.05		
2.70			0.894±0.092	0.899±0.048		
CENTRAL COLLISIONS						
Rapidity	Proton	Deuteron	π^+	π^-	K^+	K^-
0.50	37.0±0.7	5.22±0.16				
0.70	31.8±0.5	3.17±0.13	11.4±0.7	14.3±0.9	2.44±0.22	
0.90	27.8±0.5	2.39±0.12	14.7±0.7	16.1±0.8	2.53±0.33	0.587±0.102
1.10	23.5±0.4	1.60±0.10	16.4±0.5	16.9±0.5	3.17±0.39	
1.30	18.8±0.3	1.02±0.06	17.2±0.4	20.2±0.5	3.23±0.19	0.775±0.094
1.50	14.9±0.2	0.738±0.038	16.9±0.6	17.5±0.5	3.24±0.18	
1.70	11.6±0.2		15.6±0.4	15.4±0.4	2.73±0.11	0.497±0.037
1.90	9.40±0.11		12.5±0.2	12.1±0.2	2.02±0.08	
2.10	8.60±0.12		10.3±0.2	12.0±0.2	1.90±0.08	0.383±0.025
2.30			8.36±0.13	9.96±0.11		
2.50			6.71±0.12	7.58±0.10		
2.70			4.74±0.10	5.72±0.09		

TABLE II. Inverse slope parameter T (MeV) as function of the rapidity interval. The data are listed for Si+Au central and peripheral collisions. Errors quoted are statistical errors. The systematic error is estimated to be ±(10–15)% (see Sec. II G).

PERIPHERAL COLLISIONS						
Rapidity	Proton	Deuteron	π^+	π^-	K^+	K^-
0.50	106±3	89±6				
0.70	132 ± 3	118±17	134±9	140±9		
0.90	147±5	95±32	152±7	145±7	168±27	
1.10	136±6	144±78	141±5	167±9		
1.30	167±7		168±11	169±7	129±29	239±91
1.50	186±9		170±8	178±7		
1.70	190±8		151±5	151±5	221±46	
1.90	205±16		135±5	149±5		209±51
2.10	221±23		145±7	143±7	163±61	
2.30			148±9	140±7		
2.50			130±7	111±6		
2.70			133±13	134±10		
CENTRAL COLLISIONS						
Rapidity	Proton	Deuteron	π^+	π^-	K^+	K^-
0.50	144±3	163±6				
0.70	181±3	238±10	165±6	161±5	227±28	
0.90	197±3	278±17	156±5	157±4	202±21	204±56
1.10	216±4	330±27	153±4	152±4	229±17	
1.30	241±4	317±30	160±4	155±4	204±12	178±31
1.50	249±5	315±24	163±5	169±5	213±16	
1.70	244±5		160±3	172±4	242±13	177±17
1.90	238±3		166±2	159±3	190±10	
2.10	210±3		159±2	140±2	157±13	159±19
2.30			157±2	133±2		
2.50			144 ± 3	131±2		
2.70			143±3	118±2		

For K^- spectra which have low counting statistics, the systematic error can reach 20% due to variations from the rapidity binning.

III. PARTICLE DISTRIBUTIONS

A. Peripheral collisions

Multiplicity densities, dN/dy, obtained in peripheral collisions for the different particle species are shown in Fig. 13 for the Au, Cu, and Al targets. The results are approximately independent of the target which is a strong indication that the number of projectile collisions involved in peripheral collisions is small and suggests that the dynamics of the collision for large impact parameters is dominated by the primary nucleon-nucleon collisions. The distribution for protons in symmetric with respect to the nucleon-nucleon center-of-mass rapidity y_{NN}=1.72 and reaches a minimum at y_{NN} which is similar to the single nucleon-nucleon results [13] and the p+Be results [5]. Pion distributions also presented in Fig. 13, peak at the same rapidity, y_{NN}; the kaons exhibit similar behavior within the error bars.

Figure 14 shows the inverse slope parameter T in rapidity for protons and pions for the three targets. Similarly to the behavior observed for the multiplicity density, the shape of the inverse slope distribution, and the absolute values do not depend on the target. The pion slope parameters are nearly constant over two units of rapidity. The proton slope parameters are equal to the pion values at low rapidity, $y \leq 1.2$, but becomes larger than the pion values toward midrapidity. At $y = y_{NN}$ the inverse

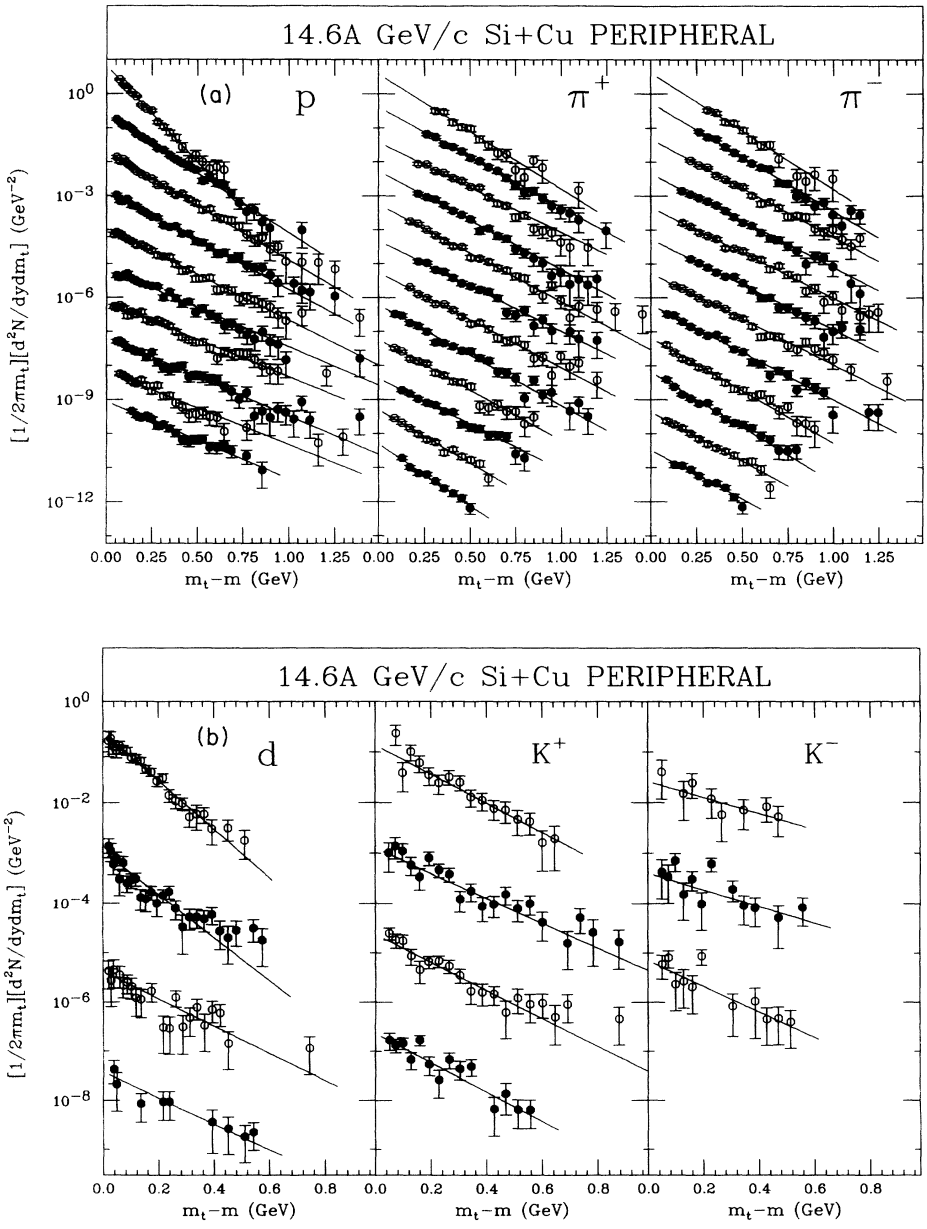

FIG. 9. (a) Invariant spectra for Si+Cu peripheral collisions. For protons, the rapidity interval is y=0.40 (top spectrum) to y=2.2 (bottom spectrum) with Δy=0.20. For pions, the rapidity interval is y=0.60 (top spectrum) to y=2.8 (bottom spectrum) with Δy=0.20. Each successive spectrum is divided by 10. Only statistical errors are shown. Systematic errors are discussed in Sec. II G. (b) Same as (a). For deuterons, the rapidity interval is y=0.40 (top spectrum) to y=1.0 (bottom spectrum) with Δy=0.20. For K^+, the rapidity interval is y=0.80 (top spectrum) to y=2.0 (bottom spectrum) with Δy=0.40. For K^-, the rapidity interval is y=1.0 (top spectrum) to y=1.8 (bottom spectrum) with Δy=0.40. Each successive spectrum is divided by 100. Only statistical errors are shown. Systematic errors are discussed in Sec. II G.

slopes are $T_\pi \simeq 150$ MeV and $T_p \simeq 200$ MeV. For comparison in $p+p$ collisions at 12 GeV/c [13] and p+Be at 14.6 GeV/c [5], the inverse slope parameters at midrapidity are $\simeq 140$ MeV for all detected particles (pions, kaons, protons). There are significant uncertainties for the kaon results and the statistics are too poor to extract meaningful systematics for the inverse slopes.

For the quasisymmetric system Si+Al it is possible to extend the rapidity range by reflecting the measured data about the center-of-mass rapidity $y_{\mathrm{c.m.}} = y_{NN} = 1.72$. This is shown in Fig. 15 for the proton and the positive pion distributions where the reflected points are solid symbols. It should be noted that for pions and protons, the measured and the reflected points agree within systematic uncertainties demonstrating consistency of the data obtained at forward angles with those from backward angles. The integrated yield for protons has been estimated by fitting the proton dN/dy distribution with a polynomial between $0 \leq y \leq 3.4$ shown in Fig. 15 (dashed line). The integrated number of protons is $\simeq 5$ in Si+Al peripheral collisions. Because of isospin symmetry, this number leads to an average of $\simeq 10$ nucleon participants involved in the peripheral collision, out of 55 possible. On the other hand, based on the kinetic energy spectra of the projectile spectators 8.2 ± 1 participants have been found for the Si+Al peripheral trigger [4]. The two methods give slightly different numbers of participants which might come from the extrapolation and assumptions made in both of them. Note that this discrepancy could also result from the contribution of rescattering of

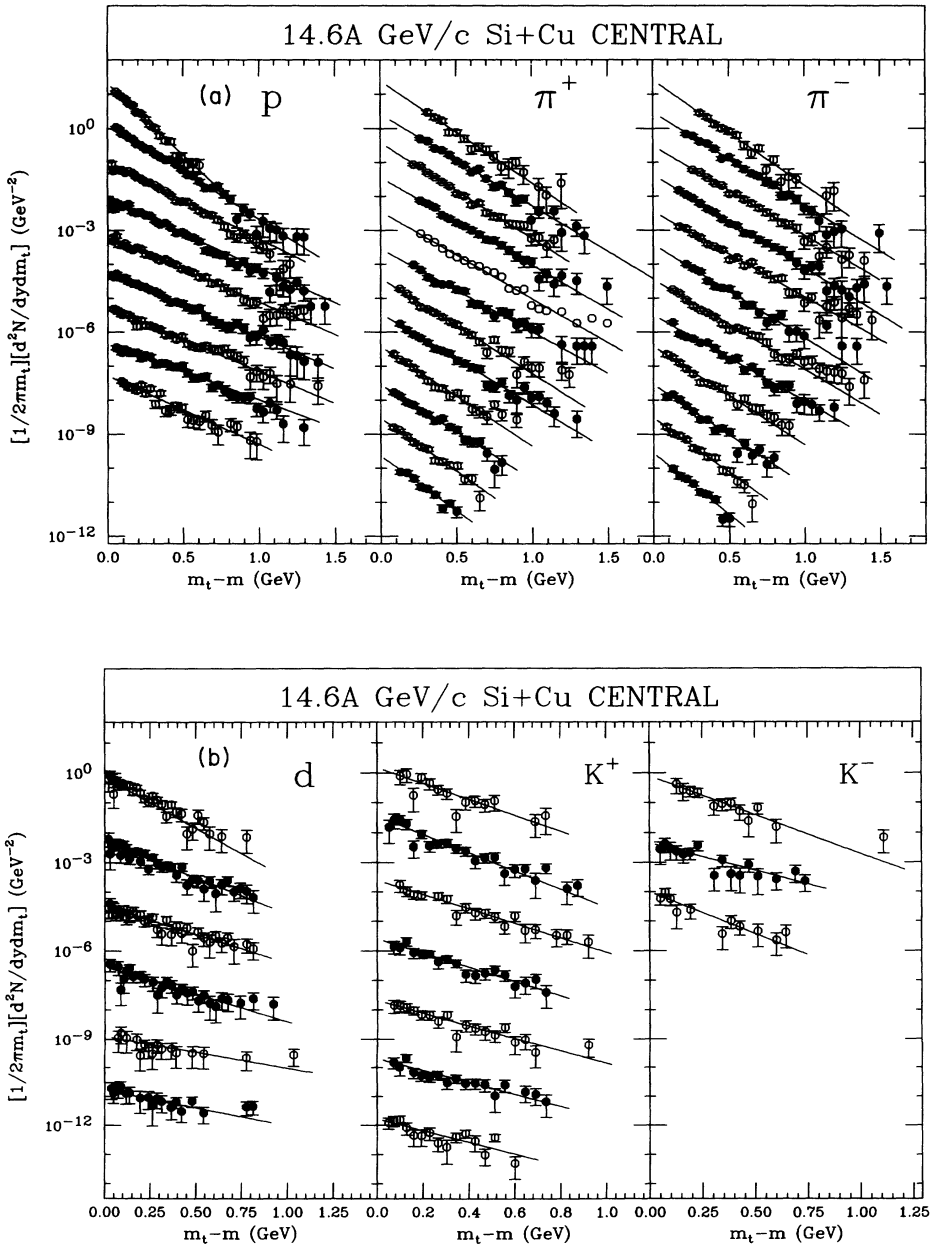

FIG. 10. (a) Invariant spectra for Si+Cu central collisions. For protons, the rapidity interval is y=0.40 (top spectrum) to y=2.0 (bottom spectrum) with Δy=0.20. For pions, the rapidity interval is y=0.60 (top spectrum) to y=2.8 (bottom spectrum) with Δy=0.20. Each successive spectrum is divided by 10. Only statistical errors are shown. Systematic errors are discussed in Sec. II G. (b) Same as (a). For deuterons, the rapidity interval is y=0.50 (top spectrum) to y=1.4 (bottom spectrum) with Δy=0.20. For K^+, the rapidity interval is y=0.60 (top spectrum) to y=1.8 (bottom spectrum) with Δy=0.20. For K^-, the rapidity interval is y=1.0 (top spectrum) to y=1.8 (bottom spectrum) with Δy=0.40. Each successive spectrum is divided by 100. Only statistical errors are shown. Systematic errors are discussed in Sec. II G.

projectile protons in the target spectators.

More insight into the peripheral data is obtained by comparing the distributions from the three targets in the same plot. This reveals some differences in the distribution between light and heavy targets. The proton and average pion multiplicity densities are shown in Fig. 16. For the proton data, the distributions for the Au and Cu targets start to rise above the Al data for the lowest rapidities ($y \leq 0.5$) probably due to the contributions from the larger number of target spectators. On the other hand, a relative π depletion, which is somewhat puzzling, appears to be observed for the Au target around midrapidity. At rapidity $y \simeq 1.4$, the ratio $\langle\pi\rangle/p$ is lower by $\simeq 30\%$ for the Au target with respect to the lighter targets.

B. Central collisions

The multiplicity density, dN/dy, corresponding to central collisions is shown in Fig. 17 for the three targets. In contrast to the peripheral collision results, the distributions show a strong target dependence. The differences are particularly dramatic for the proton distributions. In Si+Al a "targetlike" peak is observed at $y \simeq 1.0$, whereas the Si+Cu distribution seems to peak near $y \simeq 0.5$ and the Si+Au distribution continues to increase toward the target rapidity. Besides these shifts, dN/dy increases significantly with the mass of the targets below midrapidity, indicating that the number of proton participants in Si+A central collisions increases with the mass of the

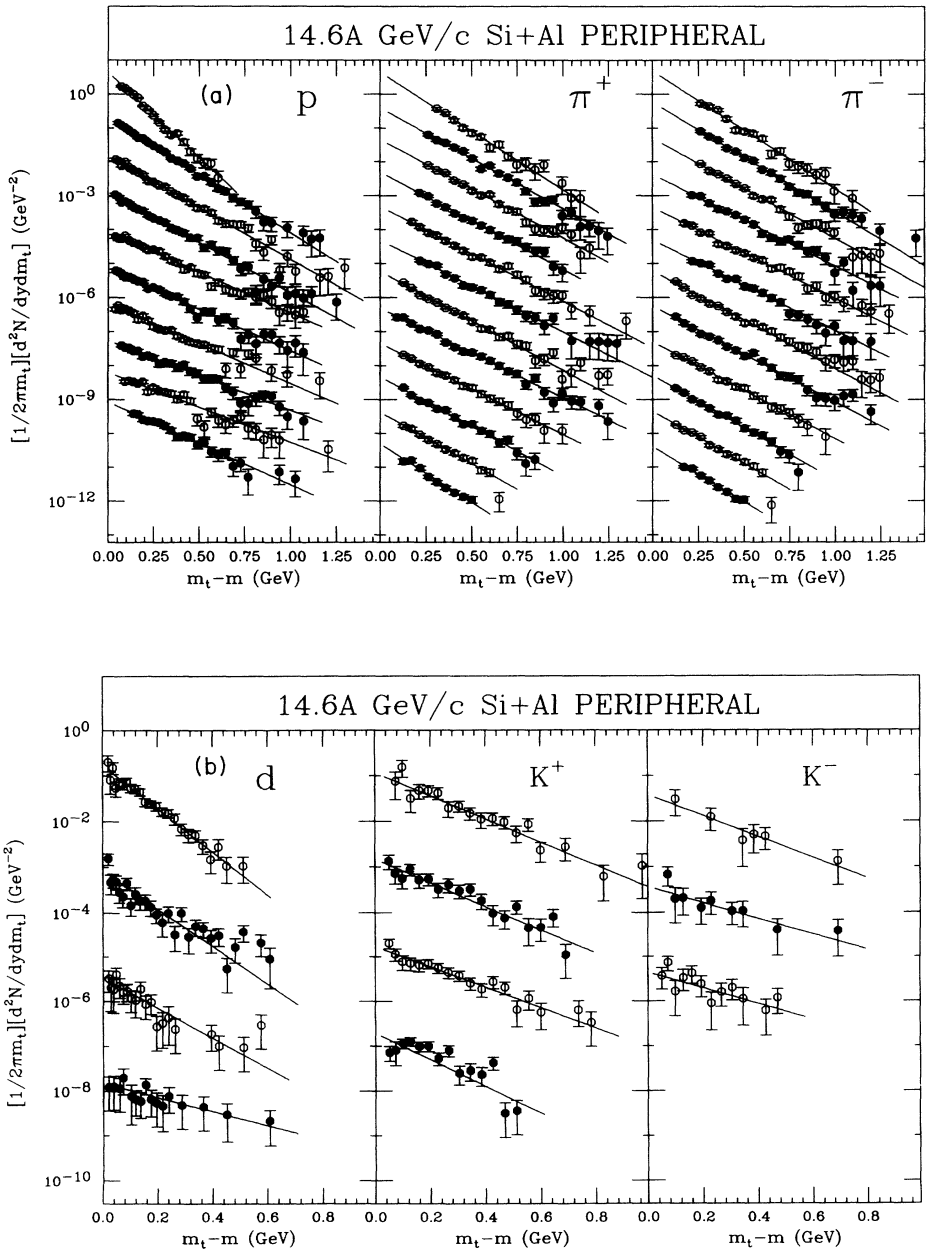

FIG. 11. (a) Invariant spectra for Si+Al peripheral collisions. For protons, the rapidity interval is y=0.40 (top spectrum) to y=2.2 (bottom spectrum) with Δy=0.20. For pions, the rapidity interval is y=0.60 (top spectrum) to y=2.8 (bottom spectrum) with Δy=0.20. Each successive spectrum is divided by 10. Only statistical errors are shown. Systematic errors are discussed in Sec. II G. (b) Same as (a). For deuterons, the rapidity interval is y=0.40 (top spectrum) to y=1.0 (bottom spectrum) with Δy=0.20. For K^+, the rapidity interval is y=0.80 (top spectrum) to y=2.0 (bottom spectrum) with Δy=0.40. For K^-, the rapidity interval is y=1.0 (top spectrum) to y=1.8 (bottom spectrum) with Δy=0.40. Each successive spectrum is divided by 100. Only statistical errors are shown. Systematic errors are discussed in Sec. II G.

target. For example, the expected total number of participants (protons and neutrons) are ≃44 in Si+Al, ≃67 in Si+Cu, and ≃100 in Si+Au. For the light systems, these numbers are calculated by assuming a geometrical overlap between the projectile participants $N_p^{\text{participant}}$ and the target (tube geometry). The number $N_p^{\text{participant}}$ is given by

$$N_p^{\text{participant}} = A_{\text{projectile}}(1 - \langle T_{\text{ZCAL}}\rangle/383) \ , \qquad (5)$$

where $\langle T_{\text{ZCAL}}\rangle$ is the average kinetic energy measured in ZCAL for the 7% cuts. For Si+Au where $\langle T_{\text{ZCAL}}\rangle$ ≃9 GeV ($\langle T_{\text{beam}}\rangle$/nucleon=13.7 GeV), the expected number of participants was calculated by assuming a full overlap between the projectile and the target with an average impact parameter of b=2 fm. Similar numbers were obtained by using Monte Carlo simulations for the reactions [14]. On the other hand, the integrated yield of participant nucleons can be obtained by fitting and integrating the dN/dy distributions in the range of $0.2 \leq y \leq 3.2$. This range is consistent with the expectation based on projectile and target Fermi momenta. The multiplicity distributions were fitted to an exponential for Si+Au and to the sum of two Gaussians for Si+Al; the number of participants is 115±10 (if neutrons ≃1.2 protons) for Si+Au central collisions and is 40±4 (if neutrons ≃protons) for Si+Al central collisions, in agreement with the previous geometric estimates.

Proton distributions are directly compared in Fig. 18 for the three targets. For a given projectile, the baryon distribution reflects the amount of "nuclear stopping" achieved in the heavy ion collision. The data show that at midrapidity (y=1.72), the multiplicity distribution increases by at least a factor of 2 from the Al target to the

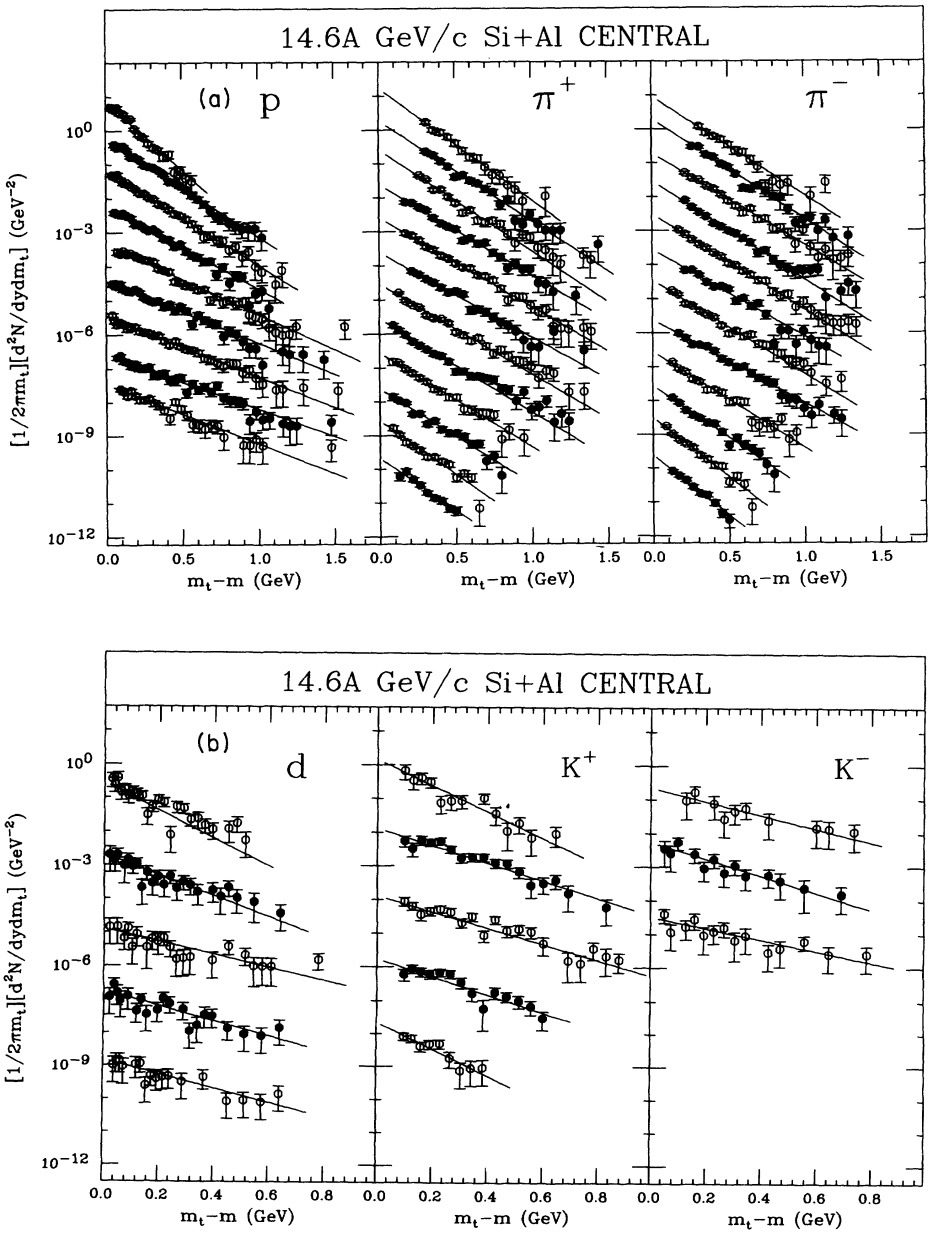

FIG. 12. (a) Invariant spectra for Si+Al central collisions. For protons, the rapidity interval is y=0.40 (top spectrum) to y=2.0 (bottom spectrum) with Δy=0.20. For pions, the rapidity interval is y=0.60 (top spectrum) to y=2.8 (bottom spectrum) with Δy=0.20. Each successive spectrum is divided by 10. Only statistical errors are shown. Systematic errors are discussed in Sec. II G. (b) Same as (a). For deuterons, the rapidity interval is y=0.50 (top spectrum) to y=1.2 (bottom spectrum) with Δy=0.20. For K^+, the rapidity interval is y=0.60 (top spectrum) to y=2.2 (bottom spectrum) with Δy=0.40. For K^-, the rapidity interval is y=1.0 (top spectrum) to y=1.8 (bottom spectrum) with Δy=0.40. Each successive spectrum is divided by 100. Only statistical errors are shown. Systematic errors are discussed in Sec. II G.

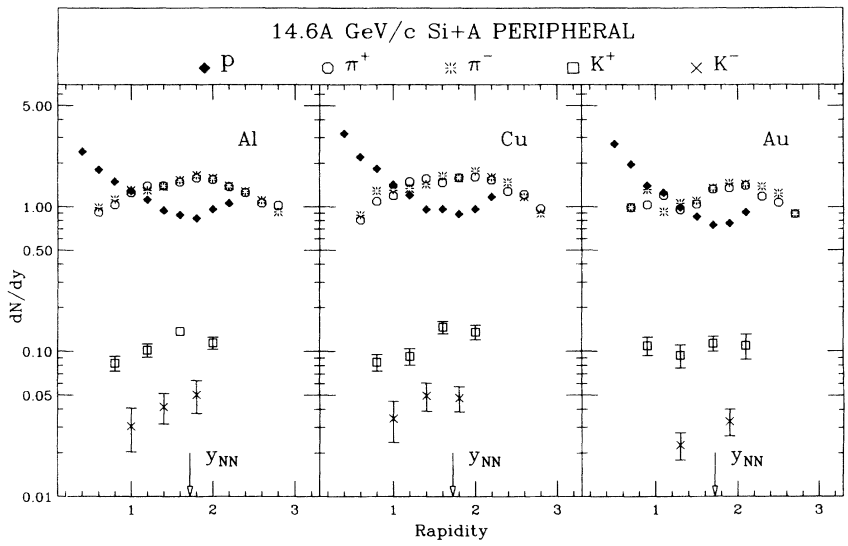

FIG. 13. Proton and meson multiplicity distributions, dN/dy, for peripheral collisions for Au, Cu, and Al targets. The rapidity of the nucleon-nucleon center of mass is shown. Only statistical errors are shown. Systematic errors are discussed in Sec. II G.

Au target. The extrapolation to higher rapidity values of the proton distribution from the Au target by an exponential (dashed line) is in agreement with data from other AGS experiments (see Sec. IV). As discussed above, the dN/dy distribution in Si+Al central collisions exhibits a "projectilelike" peak which is not seen in the extrapolation in Si+Au. Therefore, the number of protons at high rapidities ($y \geq 2.5$) is higher for Si+Al central collisions than Si+Au central collisions, signaling a lower amount of "nuclear stopping" in Si+Al than in Si+Au. The data for the Cu target seem to lie between the Au and Al data.

For the produced particles, the dN/dy shapes (Fig. 17) are broad and nearly symmetric about their maximum. The kaon distribution shapes are similar to those for pi-

TABLE III. Multiplicity density dN/dy as function of the rapidity interval. The data are listed for Si+Cu central and peripheral collisions. Errors quoted are statistical errors. The systematic error is estimated to be ±(10–15)% (see Sec. II G).

PERIPHERAL COLLISIONS						
Rapidity	Proton	Deuteron	π^+	π^-	K^+	K^-
0.40	3.19±0.08	0.275±0.017				
0.60	2.20±0.05	0.142±0.088	0.808±0.082	0.872±0.110		
0.80	1.83±0.04	0.083±0.010	1.09±0.07	1.28±0.08	0.084±0.011	
1.00	1.41±0.04	0.079±0.013	1.19±0.07	1.30±0.05		0.034±0.011
1.20	1.20±0.04		1.49±0.08	1.33±0.07	0.093±0.012	
1.40	0.954±0.039		1.56±0.06	1.43±0.06		0.050±0.011
1.60	0.960±0.036		1.46±0.08	1.63±0.08	0.146±0.015	
1.80	0.888±0.035		1.58±0.06	1.58±0.05		0.048±0.009
2.00	0.959±0.046		1.61±0.06	1.76±0.07	0.135±0.016	
2.20	1.17±0.06		1.52±0.06	1.60±0.06		
2.40			1.27±0.05	1.48±0.05		
2.60			1.21±0.05	1.16±0.05		
2.80			0.968±0.055	0.895±0.063		
CENTRAL COLLISIONS						
Rapidity	Proton	Deuteron	π^+	π^-	K^+	K^-
0.40	13.8±0.4	1.36±0.09				
0.60	15.1±0.3	1.17±0.08	6.30±0.48	6.34±0.51	1.00±0.12	
0.80	13.2±0.4	1.00±0.07	8.07±0.33	8.78±0.43	1.33±0.17	
1.00	12.6±0.4	0.906±0.081	10.8±0.4	9.70±0.42	1.86±0.18	0.544±0.076
1.20	10.7±0.3	0.697±0.370	11.8±0.5	12.9±0.4	1.93±0.17	
1.40	9.64±0.30	0.823±0.139	11.8±0.5	12.2±0.4	1.82±0.16	0.486±0.066
1.60	8.95±0.26		10.4±0.4	11.2±0.4	1.90±0.18	
1.80	8.36±0.33		11.0±0.3	11.1±0.3	1.60±0.27	0.616±0.092
2.00	8.12±0.35		10.6±0.4	10.6±0.4		
2.20			9.98±0.34	10.3±0.4		
2.40			8.16±0.33	7.50±0.40		
2.60			7.17±0.30	7.10±0.34		
2.80			5.26±0.36	5.47±0.51		

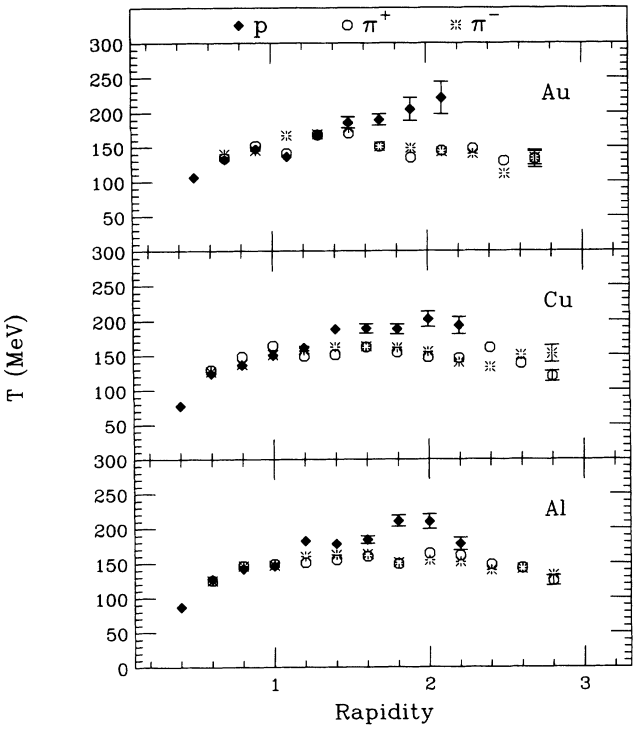

FIG. 14. Proton and pion inverse slope parameters, T, versus rapidity for peripheral collisions and for Au, Cu, and Al targets. Only statistical errors are shown. Systematic errors are discussed in Sec. II G.

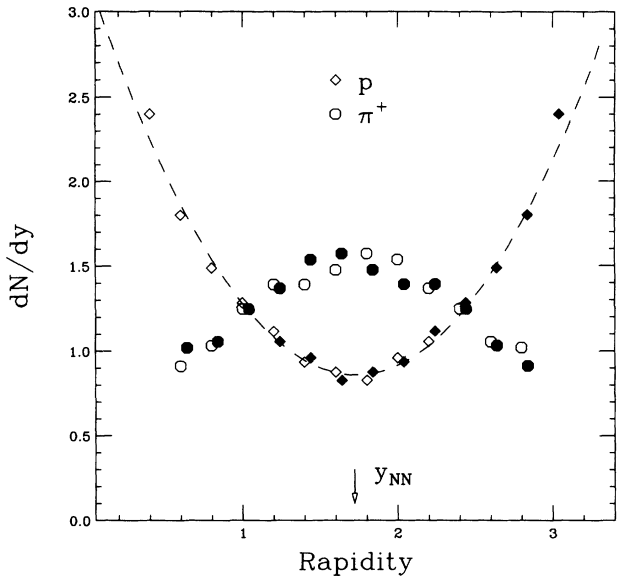

FIG. 15. Proton and pion multiplicity distributions, dN/dy, for Si+Al peripheral collisions. Solid symbols are data reflected about the center-of-mass rapidity y_{NN}. Only statistical errors are shown. Systematic errors are discussed in Sec. II G.

TABLE IV. Inverse slope parameter T (MeV) as function of the rapidity interval. The data are listed for Si+Cu central and peripheral collisions. Errors quoted are statistical errors. The systematic error is estimated to be ±(10–15)% (see Sec. II G).

PERIPHERAL COLLISIONS						
Rapidity	Proton	Deuteron	π^+	π^-	K^+	K^-
0.40	77±2	91±5				
0.60	124±2	99±10	129±8	127±7		
0.80	136±3	157±28	148±4	137±4	151±16	
1.00	150±4	165±38	164±5	151±4		275±181
1.20	161±4		149±4	157±4	172±20	
1.40	188±7		151±4	162±5		257±90
1.60	189±7		162±6	163±6	153±18	
1.80	188±7		154±5	161±4		167±37
2.00	202±11		147±5	155±4	145±17	
2.20	193±12		146±6	140±5		
2.40			161±7	133±5		
2.60			138±6	150±7		
2.80			120±8	152±12		
CENTRAL COLLISIONS						
Rapidity	Proton	Deuteron	π^+	π^-	K^+	K^-
0.40	104±3	128±7				
0.60	154±3	177±11	146±7	141±7	164±25	
0.80	195±3	224±22	161±4	159±4	176±12	
1.00	215±4	233±29	154±4	165±4	178±16	167±35
1.20	226±5	387±220	168±5	158±4	180±18	
1.40	229±6	353±121	168±5	172±4	201±25	232±38
1.60	231±7		155±7	158±6	211±33	
1.80	243±8		154±5	164±4	216±50	153±21
2.00	215±12		162±5	172±6		
2.20			148±6	150±6		
2.40			156±7	147±6		
2.60			139±6	136±7		
2.80			134±10	121±9		

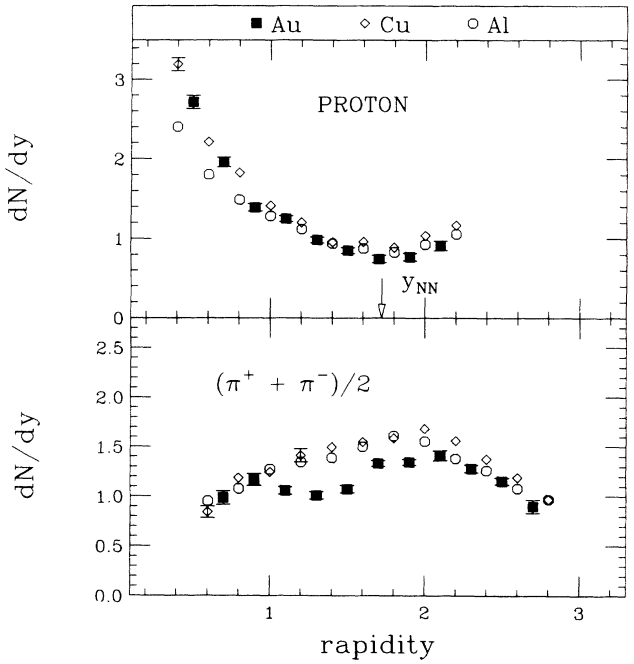

FIG. 16. Proton and average charged pion multiplicity distributions, dN/dy, for Si+Au, Si+Cu, and Si+Al peripheral collisions. The rapidity of the nucleon-nucleon center of mass is shown. Only statistical errors are shown. Systematic errors are discussed in Sec. II G.

ons. The peak position of the distribution, for both pions and kaons, shifts toward lower rapidity for heavier targets. An increase of the meson yield is also observed from the light target to the heavier target. The π^+ and π^- multiplicity distributions were fitted to a three-parameter Gaussian versus rapidity including the systematic errors. The width (σ) is found to be similar within 10% for the three targets. The parameters presented in Table VII result from Gaussian fits using σ=0.85 for all targets. The fit values of the χ^2 per degree of freedom for the three targets are in the range of 0.2–0.4. The integrated yield ratio π^-/π^+ is 1.09±0.13 in central Si+Au collisions apparently greater than unity due to the excess of neutrons for the Au target. The peak of the π^+ and π^- distributions goes from $y_{max} \simeq 1.83$ for Si+Al to $y_{max} \simeq 1.65$ for Si+Cu and $y_{max} \simeq 1.37$ for Si+Au. The ratio of the average integrated yield

$$\langle\pi\rangle = (\pi^+ + \pi^-)/2 \tag{6}$$

between the light targets and the Au target are $\langle\pi\rangle_{Al}/\langle\pi\rangle_{Au} \simeq 0.55$ and $\langle\pi\rangle_{Cu}/\langle\pi\rangle_{Au} \simeq 0.75$ which indicates that the pion multiplicity in these reactions scale roughly as the thickness of the target nucleus $A_{target}^{1/3}$. It should be pointed out that the ratio $\langle\pi\rangle_{Al}/\langle\pi\rangle_{Au}$ increases by less than 10% when the trigger cut for Si+Al is increased from the upper 7% of the interaction cross

TABLE V. Multiplicity density dN/dy as function of the rapidity interval. The data are listed for Si+Al central and peripheral collisions. Errors quoted are statistical errors. The systematic error is estimated to be ±(10–15)% (see Sec. II G).

PERIPHERAL COLLISIONS						
Rapidity	Proton	Deuteron	π^+	π^-	K^+	K^-
0.40	2.40±0.06	0.193±0.011				
0.60	1.80±0.04	0.109±0.006	0.916±0.070	0.986±0.076		
0.80	1.49±0.04	0.054±0.006	1.03±0.06	1.12±0.06	0.083±0.009	
1.00	1.28±0.03	0.055±0.014	1.25±0.06	1.30±0.05		0.031±0.010
1.20	1.11±0.03		1.39±0.06	1.30±0.07	0.102±0.010	
1.40	0.934±0.028		1.39±0.06	1.38±0.05		0.042±0.010
1.60	0.880±0.026		1.48±0.06	1.53±0.08	0.137±0.011	
1.80	0.832±0.030		1.57±0.04	1.64±0.04		0.050±0.013
2.00	0.965±0.035		1.54±0.05	1.57±0.05	0.114±0.011	
2.20	1.06±0.05		1.37±0.05	1.39±0.05		
2.40			1.25±0.04	1.27±0.04		
2.60			1.06±0.04	1.10±0.04		
2.80			1.02±0.07	0.918±0.056		
CENTRAL COLLISIONS						
Rapidity	Proton	Deuteron	π^+	π^-	K^+	K^-
0.40	5.33±0.23	0.367±0.053				
0.60	6.13±0.19	0.373±0.035	3.79±0.46	2.48±0.19	0.604±0.078	
0.80	7.26±0.19	0.389±0.070	4.93±0.30	5.39±0.31		
1.00	7.44±0.23	0.469±0.061	6.74±0.22	5.89±0.23	0.918±0.087	0.213±0.038
1.20	6.94±0.24	0.402±0.057	7.48±0.33	8.04±0.25		
1.40	6.81±0.21		8.19±0.31	8.90±0.31	0.984±0.091	0.398±0.062
1.60	6.12±0.20		8.34±0.39	9.30±0.49		
1.80	5.29±0.22		9.15±0.24	10.3±0.3	1.15±0.12	0.395±0.071
2.00	6.24±0.27		8.23±0.25	8.58±0.44		
2.20			8.00±0.35	7.87±0.31	0.889±0.126	
2.40			6.74±0.27	6.84±0.28		
2.60			6.46±0.24	6.41±0.23		
2.80			5.21±0.73	4.82±0.29		

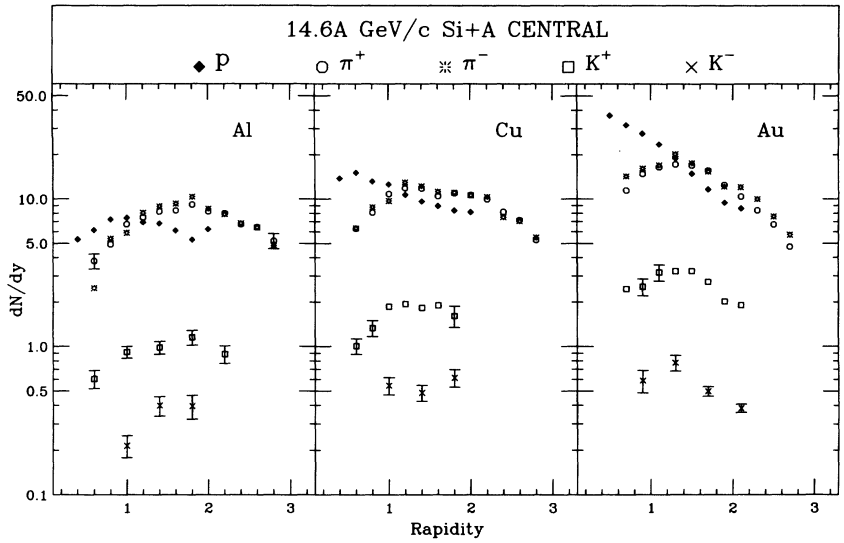

FIG. 17. Proton and meson multiplicity distributions, dN/dy, for central collisions for the Au, Cu, and Al targets. Only statistical errors are shown. Systematic errors are discussed in Sec. II G.

section to the upper 2%.

The results for the inverse slope parameter T are presented versus rapidity in Fig. 19. For protons, the inverse slope exhibits some target and rapidity dependence. The distribution reaches a maximum $T_{max} \simeq 250$ MeV near midrapidity, identically for the three systems but the maxima seem to be shifted backward as the target mass increases. For pions, the inverse slopes exhibit no target dependence and little rapidity dependence. The maximum value is $T_{max} \simeq 150$ MeV. The K^+ inverse slopes are somewhat higher than the pion inverse slopes and lower than the proton inverse slopes and are shown for

TABLE VI. Inverse slope parameter T (MeV) as function of the rapidity interval. The data are listed for Si+Al central and peripheral collisions. Errors quoted are statistical errors. The systematic error is estimated to be ±(10–15)% (see Sec. II G).

PERIPHERAL COLLISIONS						
Rapidity	Proton	Deuteron	π^+	π^-	K^+	K^-
0.40	87±2	92±5				
0.60	127±2	102±9	125±5	125±4		
0.80	142±3	129±20	146±3	146±3	172±14	
1.00	146±3	274±102	149±4	147±4		189±79
1.20	182±4		151±5	160±5	166±12	
1.40	178±6		155±4	162±5		247±97
1.60	184±6		160±5	163±6	191±18	
1.80	211±8		149±4	151±4		247±91
2.00	210±10		164±4	154±4	147±12	
2.20	178±9		161±5	152±5		
2.40			148±5	140±5		
2.60			143±6	142±6		
2.80			125±7	133±8		
CENTRAL COLLISIONS						
Rapidity	Proton	Deuteron	π^+	π^-	K^+	K^-
0.40	106±3	105±18				
0.60	149±3	140±20	132±7	150±10	112±13	
0.80	155±3	227±59	147±5	148±4		
1.00	178±4	190±29	146±5	162±5	168±11	216±61
1.20	209±5	204±40	163±4	150±4		
1.40	235±7		166±4	155±4	183±15	173±31
1.60	242±8		175±7	171±6		
1.80	267±9		163±4	158±4	165±16	257±60
2.00	246±15		157±5	177±6		
2.20			156±6	153±6	108±19	
2.40			154±6	142±6		
2.60			137±8	124±5		
2.80			140±10	123±8		

TABLE VII. Integrated yield and maximum ($N_{max} = dN/dy$ at $y = y_{max}$) of pion multiplicity distributions. The parameters result from Gaussian fits for Si+A central collisions. See text.

CENTRAL COLLISIONS-π^+			
Target	N_{max}	y_{max}	Yield
Au	16.5±1.5	1.38±0.11	33±3
Cu	12.3±1.2	1.66±0.12	25±3
Al	9.2±1.0	1.82±0.13	19±2

CENTRAL COLLISIONS-π^-			
Target	N_{max}	y_{max}	Yield
Au	18.0±1.3	1.37±0.11	36±3
Cu	12.5±1.2	1.64±0.11	26±3
Al	9.4±1.0	1.85±0.12	19±2

the three targets in Fig. 20 where the lines represent the Gaussian fits for proton (top) and pion (bottom) data found in Si+Au (Fig. 19). The results suggest that the K^+ inverse slopes increase with the target mass. The statistical uncertainties for K^- inverse slopes have been reduced by fitting the spectra over a wider rapidity range $0.5 \leq y \leq 2.2$. In Fig. 21, the K^- inverse slopes are compared with the K^+ inverse slopes for the same rapidity range where the error bars represent the linear sum of statistical errors and the estimated systematic errors due mainly to the large binning in rapidity. Whereas the statistics are too poor to draw any conclusion for Si+Al and Si+Cu, the K^- inverse slopes seem lower than those for K^+ in Si+Au.

C. Baryon distributions

As can be seen from Figs. 13 and 17, the proton distributions show, both in shape and magnitude, a strong centrality dependence. The evolution of the distribution from peripheral collisions to central collisions reflects the amount of "nuclear stopping" achieved in the central heavy ion collisions. This is shown in Fig. 22 where the proton dN/dy distributions for the quasisymmetric system Si+Al, are plotted. For central collisions, the average rapidity loss ($\delta y = y_{beam} - y_{peak}$) for projectile protons is

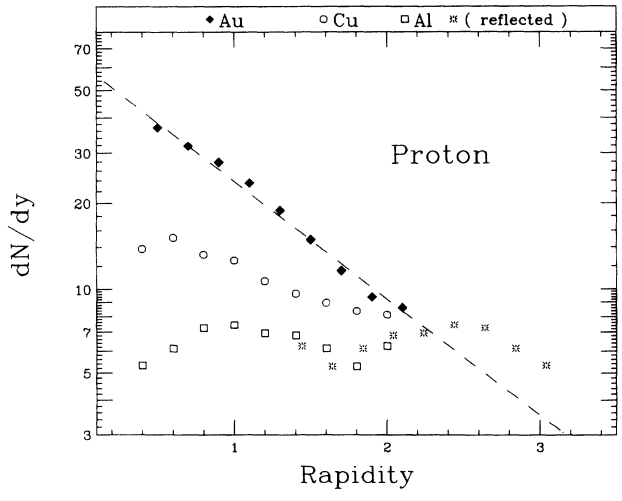

FIG. 18. Proton multiplicity distributions, dN/dy, are compared for the three targets for central collisions. The dashed line represents an exponential fit to the Si+Au proton distribution (see text for more details). Only statistical errors are shown. Systematic errors are discussed in Sec. II G.

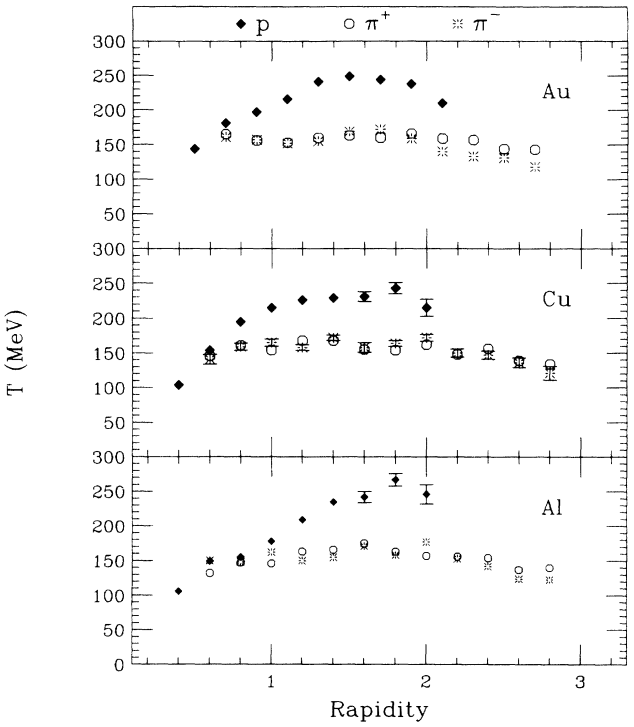

FIG. 19. Proton and pion inverse slope parameters, T, versus rapidity for central collisions and for the Au, Cu, and Al targets. Only statistical errors are shown. Systematic errors are discussed in Sec. II G.

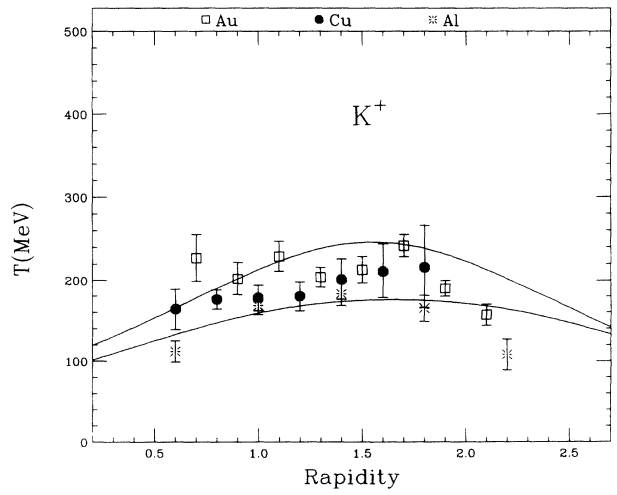

FIG. 20. K^+ inverse slope parameters, T, versus rapidity for central collisions. The lines represent the fits for protons (top) and for π's (bottom) from Si+Au data. Only statistical errors are shown. Systematic errors are discussed in Sec. II G.

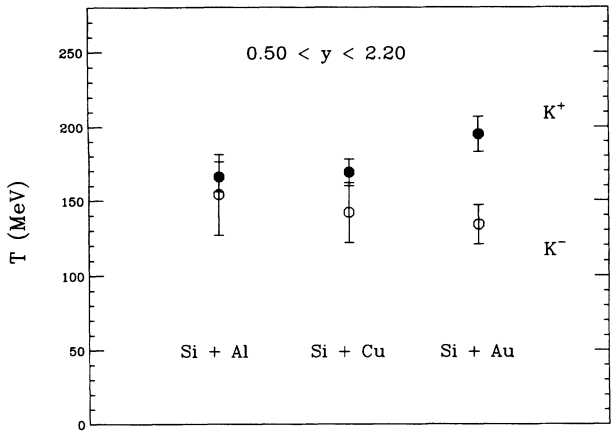

FIG. 21. K^+ and K^- inverse slope parameters for central collisions for the three targets over the rapidity range $0.50< y <2.20$. Errors bars are the sum of the statistical errors and systematic errors due to the rapidity binning.

of the order of $\delta y \simeq 1.0$; a δy=1.72 (half of the beam rapidity) corresponds by definition for symmetric systems, to "full nuclear stopping." In order to examine the influence of the centrality cut on the shape of the proton distribution, the trigger condition for Si+Al central collision was modified from the upper 7% cut to an upper 2% cut. As can been seen in Fig. 22, the 2% proton distribution is above the 7% proton distribution but they exhibit similar shapes. This suggests that the lower centrality cut for Si+Al does not increase significantly the nuclear stopping but increases the total number of participants. As already mentioned, the amount of "nuclear stopping" is higher for the heavier targets and it therefore follows that δy for proton participants is $\geq$1.0 for Si+Au (and Si+Cu) central collisions. It has been shown that

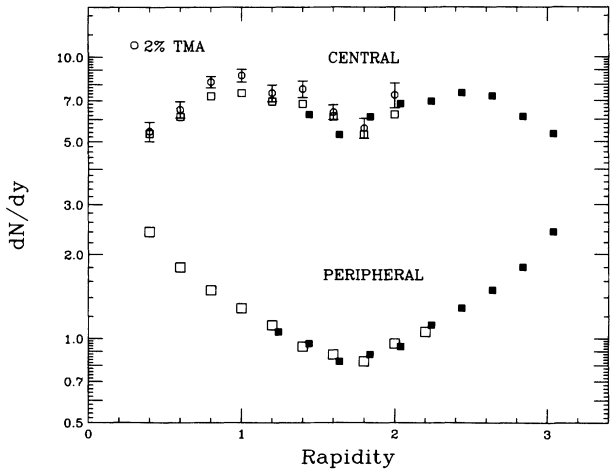

FIG. 22. Proton multiplicity distributions dN/dy for Si+Al peripheral and central (7%) collisions. Solid symbols are data reflected about the center-of-mass rapidity. Errors bars are not shown for solid symbols. Proton dN/dy for the 2% central cut are also shown (octagons). Only statistical errors are shown. Systematic errors are discussed in Sec. II G.

the centrality of the collision significantly modifies the maximum value of the inverse slope parameter achieved around midrapidity, $T_{\max} \simeq$200 MeV for peripheral collisions and $T_{\max} \simeq$250 MeV for central collisions.

Emission of deuterons in heavy ion collisions at lower energies [15] has been described successfully by the coalescence model [16]. Therefore, the results for the deuteron production were compared with the proton data. In Fig. 23, the d/p^2 multiplicity ratios are shown, versus rapidity, for both peripheral and central collisions. As clearly seen from the figure, the ratio d/p^2 is almost independent of the rapidity which is consistent with the coalescence picture. While the ratio is independent of the target in peripheral collisions, the ratio is lower for the heavier targets in central collisions. Further, the ratio is higher in peripheral collisions than in central collisions. The centrality dependence and the target dependence of the ratio d/p^2 suggest that deuteron production is sensitive to the size of the participant region in agreement with the coalescence mechanism. According to this mechanism, the differential invariant multiplicity for deuterons can be expressed as

$$E_d(d^3N_d/dp_d^3) = a * E_p(d^3N_p/dp_p^3) * E_n(d^3N_n/dp_n^3) \ , \tag{7}$$

where a is in GeV^2. It is then assumed that the neutron spectra are identical to those of protons. From the above equation and by using a thermal model, one can estimate the size of the interaction region. First, the factor a is determined from the deuteron invariant spectra divided by the squared proton invariant spectra at momenta $2p_{\text{proton}}$. The coalescence radius $\tilde{p}_0$ is given by [17]

$$\tilde{p}_0 = (mZ_{\text{tot}}a/2\pi N_{\text{tot}})^{1/3} \ , \tag{8}$$

where Z_{tot} and N_{tot} are, respectively, the proton and neutron numbers and m is the mass of the nucleon. The thermal model [17] relates the volume of the participant region V to the coalescence radius $\tilde{p}_0$ as

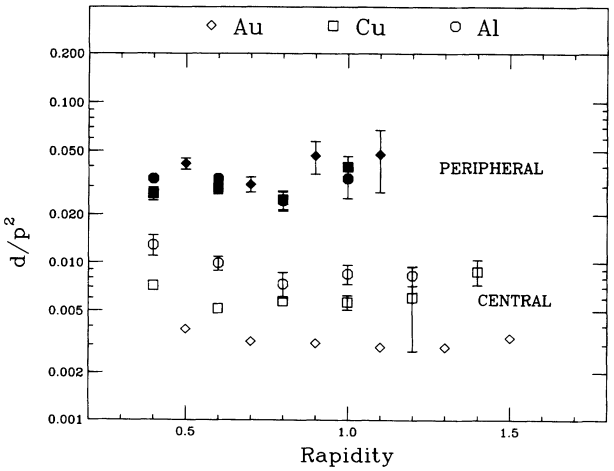

FIG. 23. Ratio d/p^2 versus rapidity for Si+A central and peripheral collisions.

TABLE VIII. Equivalent radii (size of interaction region) for Si+A collisions. The values were calculated from deuteron and proton data. See text.

Target	Radii (fm) of the participant volume Peripheral	Central
Al	4.6±0.4	5.7±0.3
Cu	4.5±0.4	6.7±0.3
Au	4.1±0.4	7.9±0.2

$$V = (3h^3/4\pi\tilde{p}_0^3)e^{E_0/kT_0} , \quad (9)$$

where E_0 is the binding energy of the deuteron. From the two last equations and assuming $E_0 \ll kT_0$, the radius R of the equivalent sphere can be written as

$$R = (N_{\rm tot}9\pi^2\hbar^3/mZ_{\rm tot}a)^{1/3} . \quad (10)$$

The radii of the equivalent spheres are reported in Table VIII for peripheral collisions and central collisions and show within statistical error bars no rapidity dependence. The values reported in Table VIII were calculated for the entire rapidity coverage shown in Fig. 23. As expected, the radius increases from peripheral to central collisions where the maximum is obtained for the Au target. It is found that these radii are larger than the radius of the projectile for central collisions. However a uniform thermal model, assuming uniform spherical symmetry in particular may be inadequate for the description of these collisions. These coalescence results can be compared with two-particle correlation data which provide additional information about the dynamics of the collisions. The E-802/859 experiment [18] has two-particle correlation data for K^+, π^+, π^-, and protons [19]. The results are significantly different. For Si+Au central collisions, the source radii defined as the Lorentz corrected rms radii are (3.22±0.37) fm for K^+, (3.93±0.28) fm for π^+, and (4.50±0.14) fm for protons in comparison with (6.12±0.15) fm obtained from the coalescence analysis [rms=$(3/5)^{1/2} * R$ for a sphere]. Inverse slope parameter ratios T_d/T_p shown in Fig. 24 are ≃1 for both peripheral and central collisions. Deviations occur only for the Au target where the ratio seems to become larger.

D. Meson production

The pion and kaon rapidity distribution shapes do not depend significantly on centrality, whereas the yield of these particles increases as the impact parameter decreases reflecting the number of participants involved in the collision. The total number of pions $\pi_{\rm tot}$ produced in the reaction can be calculated as a function of the expected number of participants (see Sec. III B). By assuming that $\pi^0 = (\pi^+ + \pi^-)/2$ and from the values given in Table VII, $\pi_{\rm tot} \simeq (1.2 \pm 0.2) * N_{\rm participant}$ for peripheral collision, similar to $\pi_{\rm tot} \simeq (1.1 \pm 0.2) * N_{\rm participant}$ obtained in central collisions.

The observed strangeness enhancement in heavy ion collisions [3,4] has been proposed as a signal for the quark-gluon plasma, although cascade models [20,21] have reproduced this enhancement by introducing rescattering of produced particles in hadronic matter. In Fig. 25, the K^+/π^+ multiplicity ratios versus rapidity are compared for peripheral and central collisions for the three targets. For peripheral collisions, the ratios are the same within errors for the three targets (≃8%) and are independent of rapidity. The value of ≃8% is also consistent with the value of 4–8 % measured in $p+p$ reactions at similar energies [22] and those measured in p+Be at the same energy [5]. For central collisions, the ratio increases from the lightest target to the heaviest target. The ratios are also independent of the rapidity within $0.5 \leq y \leq 2.3$. The ratio reaches a mean value over that rapidity range of $K^+/\pi^+ = (18.5 \pm 0.7)\%$ for Si+Au, $K^+/\pi^+ = (16.3 \pm 0.6)\%$ for Si+Cu, and $K^+/\pi^+ = (13.0 \pm 0.8)\%$ for Si+Al. In general, from peripheral collisions to central collisions the K^+/π^+ multiplicity ratio increases by a factor of 2–3. A more detailed description of this centrality dependence has been published in Ref. [4]. Note that for p+Au reactions [5], the K^+/π^+ multiplicity ratio is ≃12% over a similar ra-

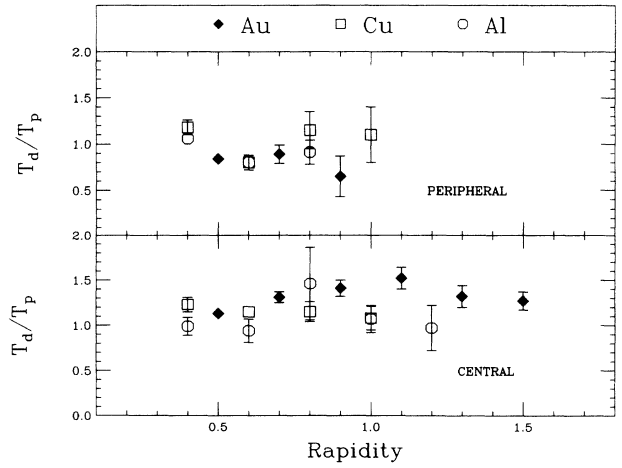

FIG. 24. Inverse slope parameter ratios for protons and deuterons versus rapidity for Si+A central and peripheral collisions.

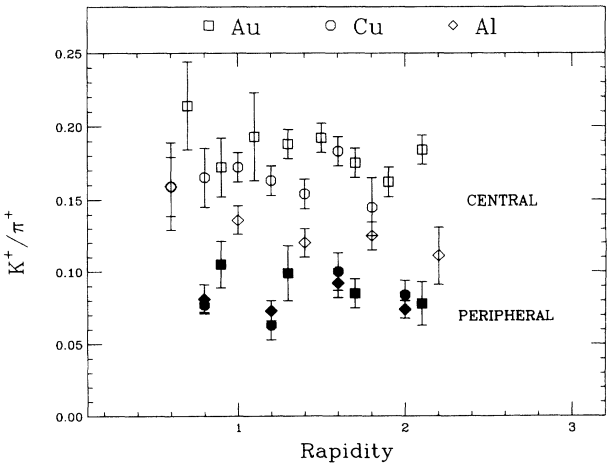

FIG. 25. Multiplicity density ratio, K^+/π^+, versus rapidity for Si+A central and peripheral collisions.

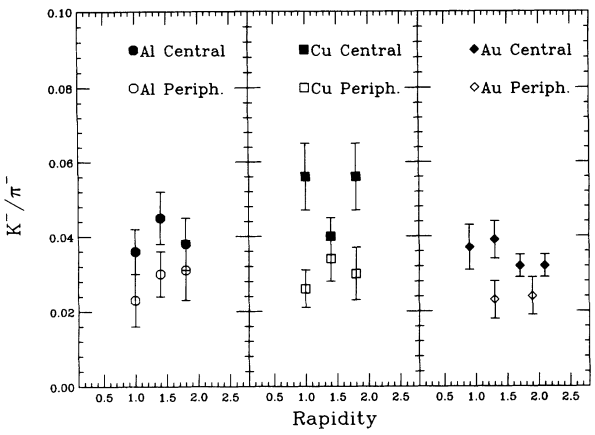

FIG. 26. Multiplicity density ratio, K^-/π^-, versus rapidity for Si+A central and peripheral collisions.

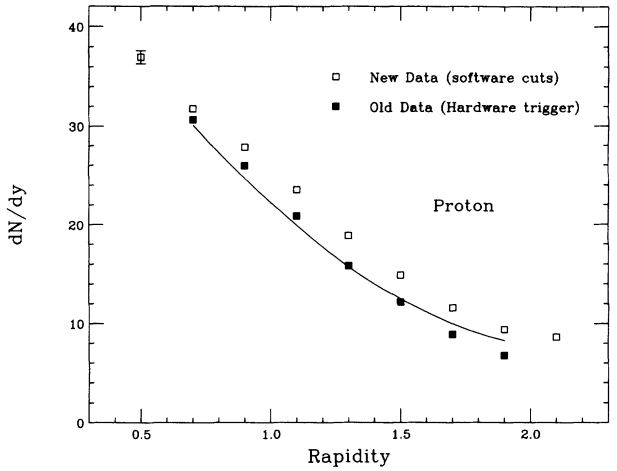

FIG. 27. Comparison of Si+Au central collision proton data from this paper and E-802 proton data from Ref. [25]. The line shows the effect of applying the old hardware trigger to the new data. See text.

pidity interval. The measured ratio for Si+Al in central collisions is identical within error bars with the recent multiplicity ratio K^+/negatives measured in central S+S reactions at CERN [23] demonstrating the weak dependence of the K^+/π^+ multiplicity ratio with the energy in the center of mass ($\sqrt{s}$=5.4 GeV at AGS and $\sqrt{s}$=19.4 GeV at CERN).

The K^-/π^- multiplicity ratio for the various targets is shown in Fig. 26 for central and peripheral triggers. The peripheral collision data are in rough agreement with p+p data [24] which include large uncertainties and with the p+Be data [5] where $K^-/\pi^- \simeq 0.025$. It is seen in Fig. 26 that despite uncertainties, the K^-/π^- multiplicity ratios for central collisions are systematically higher than the ratios obtained in peripheral collisions. As is the case for K^+ production, the K^- yield seems to increase with centrality. The K^+/K^- multiplicity ratio shows, within error bars, little impact parameter dependence. The value of this ratio for central collisions measured in the rapidity interval, $1.0 \leq y \leq 2.0$, is $K^+/K^- \simeq 4.0 \pm 0.7$ for all three targets.

IV. CONSISTENCY WITH EARLIER E-802 DATA AND OTHER AGS EXPERIMENTS

Data from central Si+Au interactions have been published previously by the E-802 Collaboration [3,25]. The present π^+, π^-, and K^- multiplicities are systematically higher than the previous results by 5–15 %, depending on rapidity. For rapidities $y \leq 1.0$ the present K^+ results are below the older data and the increase in K^+ multiplicity toward y=0.5, reported in Ref. [25], is not observed here (see, e.g., Fig. 17). The present proton results, the open squares in Fig. 27, are systematically higher than the earlier data (solid squares), the difference is ≈5% for $y \simeq 0.7$ increasing to ≈40% near y=2.0.

For the pions and kaons, the differences between old and new data are within the systematic errors, and can be traced to the changes in software cuts and particle identification acceptances discussed in Sec. II. For protons, part of this difference originates in the change in analysis procedure, but here in addition the trigger conditions play a major role. The previous data were triggered with a hardware cut in multiplicity that leads to a trigger cross section of roughly 7% of the interaction cross section; the present data have a sharp cut in multiplicity at 7% set in software. The proton distribution obtained from the new data with a hardware multiplicity trigger set close to the old prescription and analyzed with the new procedures is shown in Fig. 27 as the fully drawn curve. Only for the y=1.7 and y=1.9 points does a significant difference remain, caused mainly by the large extension of proton particle identification towards higher momenta used in the new analysis.

Experiment E-810 has published Si+Au results [26,27] for negative particles and for the difference between positive and negative particles. The E-810 trigger condition was a charged multiplicity above 60 for pseudorapidities $\eta \geq 1.55$. The top half of Fig. 28 shows a positive minus negative comparison of the E-810 results and E-802 results for a software trigger than simulates the E-810 trigger, which is less central than the 7% trigger used here. The agreement is good. The lower panel of Fig. 28 shows a comparison between the negatives from the two experiments, again under the E-810 trigger conditions. Here the E-802 data have been multiplied by 1.25 before comparing the data. The E-810 spectra for negatives (mostly π^-) show two experimental components at these rapidities, a very steep one at low m_t and a second, flatter component at $m_t \geq 100$ MeV. The factor 1.25 corresponds closely to the contribution from the steep low m_t component, not observable in the E-802 m_t acceptance, and therefore not included in the single exponential fits

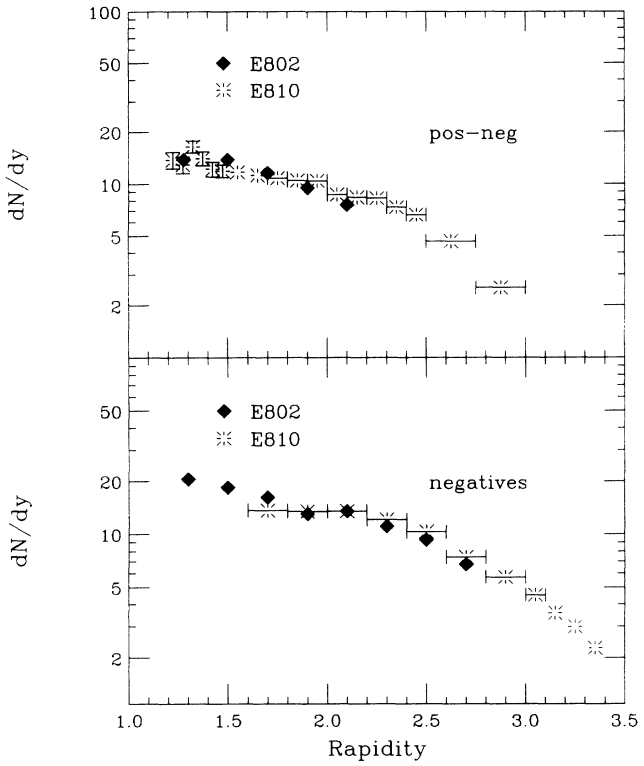

FIG. 28. Comparison of E-802 data and E-810 data (Refs. [26,27]) for Si+Au central collisions. Note the central trigger requirement here is different from the E-802 7% cut for both experiments: charged multiplicity > 60 for $\eta > 1.55$. The E-802 negative data in the lower panel are multiplied by 1.25. See text for more information.

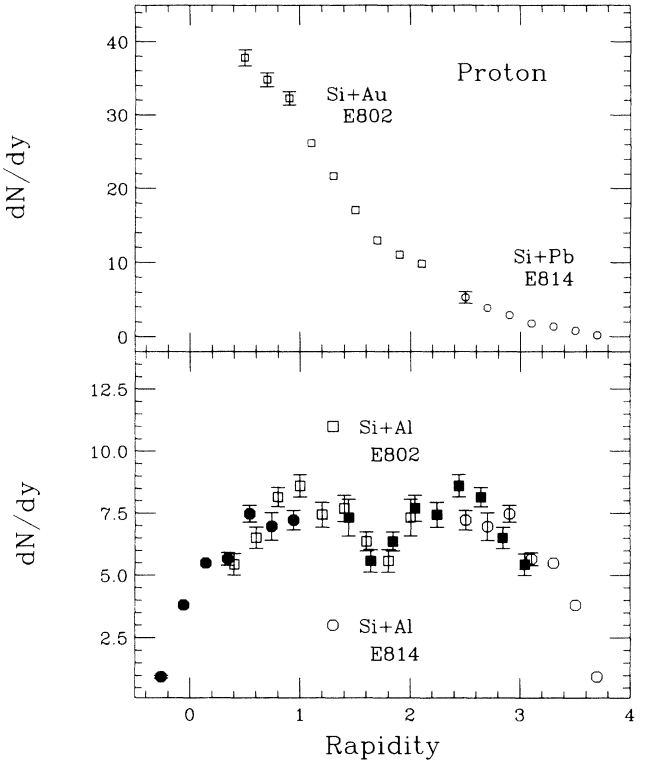

FIG. 30. Comparison of E-802 proton data and E-814 proton data for central collisions. E-802 data have multiplicity cuts (2%) for Si+Au and Si+Al while E-814 data have a total transverse energy cut (2%) for Si+Pb (Ref. [29]) and a multiplicity cut (0.2%) for Si+Al (Ref. [28]). The solid points have been reflected about central rapidity for Si+Al.

used for the E-802 analysis.

Kaon production can be compared for central Si+Al (E-802) and central Si+Si (E-810 $\sigma_{\text{trig}} \simeq 8\%\ \sigma_{\text{int}}$), as shown in Fig. 29. The data were reflected about midrapidity and plotted again as the solid symbols, extending the data to higher rapidities for E-802 and to lower rapidities for E-810. The collision systems have rough isospin symmetry and hence kaon production satisfies

$$2K_s^0 \simeq K^- + K^+ \ . \tag{11}$$

The agreement between the two experiments is very good.

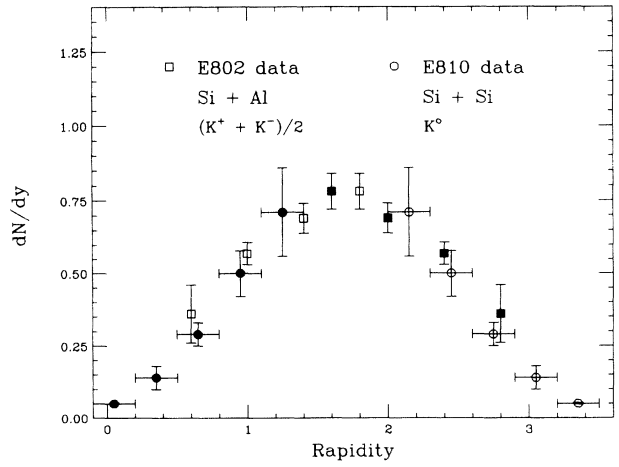

FIG. 29. Comparison of E-802 data and E-810 (Refs. [26,27]) data for the kaon production in central collisions for light systems. Data were reflected about midrapidity (solid symbols).

Figure 30 offers a comparison between the present data for protons, from Si+Au and Si+Al and results from experiment E-814 on Si+Pb and Si+Al (Refs. [28,29]). The top part of the figure shows E-802 results with a software cut at the upper 2% of the TMA distribution, while the E-814 trigger was the upper 2% of total transverse energy. Multiplicity and transverse energy are known to be correlated quantities [30], so the triggers are comparable. While the two experiments have no overlap in rapidity, the two data sets seem to join quite smoothly, and without any pronounced projectilelike proton peak.

For Si+Al (lower part of the figure) both experiments have triggers set on charged particle multiplicity, but the E-802 statistics do not allow a cut at 0.2% as used by E-814. The E-802 results are quite stable toward small variations in the multiplicity cut (from 7% to 2%); the good overlap between the E-802 data (squares) and the E-814 data (octagons) signals reasonable agreement between the two experiments.

V. ENERGY AND MOMENTUM BALANCE IN THE COLLISION

Energy and momentum conservation provide a global consistency test for the data. To apply such a test the data must be extrapolated to the full phase space and supplemented via baryon and charge conservation for estimates of the neutral and unobserved particles. Such a test therefore suffers from extrapolation errors.

The method chosen is illustrated below for Si+Au central collisions. The total average energy $\langle E\rangle_{\rm tot}$ is given by

$$\langle E\rangle_{\rm tot} = \sum_{\rm particles} \int (dN/dy)\langle m_t\rangle \cosh(y) dy \ , \qquad (12)$$

and for the total average longitudinal momentum $\langle p_L\rangle$,

$$\langle p_L\rangle_{\rm tot} = \sum_{\rm particles} \int (dN/dy)\langle m_t\rangle \sinh(y) dy \ . \qquad (13)$$

The sum over all particles can be approximately reduced to the sum over species of hadrons including protons, neutrons, deuterons, pions, kaons, and strange baryons.

The following assumptions have been made to take into account the particles not detected by the spectrometer. The total number of kaons is given by the relation $n_K = 2.43 * n_{K^+}$ by taking the experimental K^-/K^+ ratio and by assuming that $n_{K_0} + n_{\bar{K}_0} = n_{K^-} + n_{K^+}$. The number of strange baryons is assumed to be $2 * n_{K^+}$, although part of the strange baryon decay products might already be accounted for in the proton and meson distributions. The total number of pions is $n_\pi = 3 * n_{\pi^+}$ assuming $\pi^+ = \pi^- = \pi^0$. The relativistic cascade code ARC which reproduced the $(p+d)$ multiplicity distribution in Si+Au [21], has been used to estimate the n/p ratio as a function of rapidity. This ratio can be parametrized as

$$n/p \simeq 1.50 - 0.63y + 0.31y^2 - 0.046y^3 \ . \qquad (14)$$

Finally, the conservation of the charge and baryon number gives an estimation of the number of target spectator nucleons (y=0). All the distributions are integrated from y=0 to y=3.5. Therefore extrapolations are required for the lowest and highest rapidity ranges. The proton and deuteron multiplicity distributions are fitted as $a_0 e^{-b_0 y}$ with (a_0=65.3, b_0=0.95) for protons as can be seen in Fig. 18 and (a_0=14.9, b_0=1.96) for deuterons. The inverse slope parameters T (Fig. 18) are fitted as $T_0/\cosh(y-y_0)$ with (T_0=246 MeV, y_0=1.60) for protons and (T_0=320 MeV, y_0=1.60) for deuterons. They define $\langle m_t\rangle$ as

$$\langle m_t\rangle = (m^2 + 2mT + 2T^2)/(m+T) \ . \qquad (15)$$

The meson multiplicity distributions are fitted as $a_0 e^{-(y-y_0)^2/2\sigma^2}$ with (a_0=16.7, y_0=1.40, σ=0.82) for π^+ and (a_0=3.19, y_0=1.50, σ=0.74) for K^+. The parameter T is fitted to the function $104[1/\cosh(y-1.00) + 1/\cosh(y-2.20)]$ for π^+ (Fig. 19) and $210/\cosh(y-1.50)$ for K^+. Note that this extrapolation excludes contribution from any low additional m_t component in the spectrum. By assuming an identical rapidity dependence for all pions (π^-, π^+, and π^0) the contribution of the low m_t component could reach $\simeq$10% of $\langle E\rangle_{\rm pions}$ and $\simeq$10% of $\langle p_L\rangle_{\rm pions}$ based on the E-810 data [26]. The results concerning the energy and momentum balance are given in Table IX for each particle specie. The total average energy reaches $590 \pm 20_{\rm fit} \pm 35_{\rm syst}$ GeV, and for the total longitudinal momentum $413 \pm 19_{\rm fit} \pm 41_{\rm sys}$ GeV/c. The incident energy and momentum being 594 GeV and 409 GeV/c, respectively, conservation of energy and momentum are achieved within errors in the reaction ruling out any need for nuclear transparency in central Si+Au collisions [31]. In fact, the agreement is better than the systematic errors on $\langle E\rangle_{\rm tot}$ and $\langle p_L\rangle_{\rm tot}$. The authors of Ref. [31] have overstated the deviations from the data necessary to imply transparency and have misunderstood the meaning of systematic errors. The results concerning only the measured quantities, without extrapolation in transverse mass m_t and rapidity y, are given in Table X. As can be seen only about $\frac{1}{4}$ of the available energy and momentum is within the E-802 acceptance and the conclusion regarding transparency depends on the choice of extrapolation. The extrapolation used here is consistent with the E-814 [29] and E-810 [27] data.

TABLE IX. Energy and momentum balance for Si+Au central collisions. The data were extrapolated to the full phase space. See text.

	$\langle E\rangle$ (GeV)	$\langle p_L\rangle$ (GeV/c)
Protons	186	124
Neutrons	226	138
Deuterons	21	11
Pions	108	96
Kaons	27	24
Strange baryons	22	20
TOTAL	590	413

VI. SUMMARY AND REMARKS

Baryon and meson distributions were studied in central and peripheral ultrarelativistic heavy ion collisions. The centrality of the collision was selected with a target multiplicity array and a zero degree calorimeter. Results are presented for a Si beam at 14.6A GeV/c corresponding to a nucleon-nucleon center-of-mass energy of $\sqrt{s}$=5.4

TABLE X. Measured energy and momentum for Si+Au central collisions.

	$\langle E\rangle$ (GeV)	$\langle p_L\rangle$ (GeV/c)
Protons	77	63
Deuterons	8	6
π^+	24	23
π^-	28	25
K^+	7	6
K^-	1	1
TOTAL	147	124

GeV and targets of Al, Cu, and Au. The E-802 spectrometer provided particle identification and momentum determination for protons, deuterons, charged kaons, and charged pions.

Strong target mass dependence was found for the multiplicity density in central collision results. This is not the case for the peripheral collisions suggesting that the dynamics of large impact parameter collisions is dominated by a superposition of primary nucleon-nucleon collisions. The proton distribution in central collisions is very sensitive to the mass of the target and this dependence indicates that the total number of participants in the collision and the amount of "nuclear stopping" of the reaction increases with the target mass. The proton distributions show that the average rapidity loss for a projectile nucleon is $\delta y \simeq 1.0$ for Si+Al central collision and larger for heavier targets. Indeed a correlation exists between the proton rapidity distribution and the pion production: the higher amount of "nuclear stopping" for the heavier target is associated with an increase in pion multiplicity. The pion distributions shift toward lower rapidity values for the heavier targets and the average multiplicity scales as $\simeq A_{\text{target}}^{1/3}$. This is in contrast to the minimum bias $p + A$ results [5] where the average pion multiplicities do not increase significantly with the target mass.

Strong dependence on centrality was found for the d/p^2 multiplicity ratio, in particular for the Au target, probably due to different sizes of the participant region. In comparison to the coalescence measurement, the two-particle correlation measurements show smaller radii for the size of the participant region. This could be due to the fact that the coalescence results are very model dependent and/or to different dynamics for the production and absorption of each particle specie.

An enhancement of the K^+/π^+ multiplicity ratio by a factor of $\simeq$2–3 is observed from peripheral collisions to central collisions, being larger for the heavier mass target. The results for K^- indicate similar enhancement with centrality for the K^-/π^- multiplicity ratios. The K^+/π^+ and K^-/π^- ratios are independent, within errors, of the rapidity values for $0.5 \leq y \leq 2.0$.

The *inverse slope distributions* exhibit roughly a Gaussian shape versus rapidity for the three targets. For protons, the inverse slope parameter distribution has a maximum value for central collisions at $T_{\max} \simeq 250$ MeV, identically for the three targets, suggesting that $T_{\max}$ is independent of the target mass. The distributions reach a maximum $T_{\max} \simeq 200$ MeV for peripheral collisions. Several mechanisms such as elastic and inelastic proton scattering, rescattering of produced particles and collective effects are possible explanations for the increase of proton inverse slopes in central collisions. Quite different from protons, the maximum inverse slope parameter for pions shows no centrality dependence with $T_{\max} \simeq 150$ MeV for the three targets. This might be due to the fact that the decay of baryon resonances produced with large cross sections do not significantly modify the high energy tail of the pion transverse mass distribution [32]. The K^+ inverse slopes in central collisions are generally lower than those of protons but higher than those of pions. In Si+Au central collisions, the K^+ inverse slope parameters seem to be larger than the K^- inverse slopes which could be due to different rescattering cross sections.

Energy and momentum balance in the reactions is verified based on reasonable extrapolations of the E-802 data. The data presented in this paper are in excellent agreement with data published by the E-810 and E-814 collaboration when the different sets of data are compared with similar centrality triggers.

ACKNOWLEDGMENTS

The authors would like to thank the Tandem and AGS staffs for providing the silicon beam. This work has been supported by the U.S. Department of Energy under contracts with ANL (W-31-109-ENG-38), BNL (DE-AC02-76CH00016), Columbia University (DE-FG02-86-ER40281), MIT (DE-AC02-76ER03069), U.S. Riverside (DF-FG03-86ER40271), and by NASA (NGR-05-003-514), under contract with the University of California, and by the U.S.-Japan High Energy Physics Collaboration Treaty.

[1] J. Rafelski and B. Muller, Phys. Rev. Lett. **48**, 1066 (1982).
[2] E-802 Collaboration, T. Abbott *et al.*, Nucl. Instrum. Methods **A290**, 41 (1990).
[3] E-802 Collaboration, T. Abbott *et al.*, Phys. Rev. Lett. **64**, 847 (1990).
[4] E-802 Collaboration, T. Abbott *et al.*, Phys. Lett. B **291**, 341 (1992).
[5] E-802 Collaboration, T. Abbott *et al.*, Phys. Rev. D **45**, 3906 (1992).
[6] E-802 Collaboration, T. Abbott *et al.*, Phys. Rev. C **44**, 1611 (1991).
[7] E-802 Collaboration, T. Abbott *et al.*, Phys. Rev. C **45**, 2933 (1992).
[8] C. G. Parsons, Ph.D. thesis, M.I.T., 1992.
[9] R. Brun *et al.*, GEANT user guide, Report DD/EE/84-1, CERN 1987.
[10] V. A. Vutsadakis, Ph.D. thesis, M.I.T., 1992; J. C. Costales, Ph.D. thesis, M.I.T., 1990.
[11] B. A. Cole, Ph.D. thesis, M.I.T., 1992.
[12] MINUIT reference manual, version 92.1, D506 CERN 1992.
[13] V. Blobel *et al.*, Nucl. Phys. **B27**, 285 (1971).
[14] H. Z. Huang, Ph.D. thesis, M.I.T., 1990; M. A. Bloomer, Ph.D. thesis, M.I.T., 1990.
[15] S. Nagamiya and M. Gyulassy, Advances in Nuclear Physics (Plenum, New York, 1984), Vol. 13; R. Stock, Phys. Rep. **135**, 259 (1986).
[16] S. F. Butler and C. A. Pearson, Phys. Rev. **129**, 836 (1963).
[17] J. Gosset *et al.*, Phys. Rev. C **16**, 629 (1977); A. Z. Mekjian, Phys. Rev. Lett. **38**, 640 (1977); Phys. Rev. C **17**, 1051 (1980); M. C. Sarabura, Ph.D. thesis, M.I.T., 1989.
[18] E-802 Collaboration, T. Abbott *et al.*, Phys. Rev. Lett.

69, 1030 (1992); Y. Akiba *et al.*, *ibid.* **70**, 1057 (1993).
[19] E-802 Collaboration, G. S. F. Stephans *et al.*, *QM'93 Proceedings*, Borlange 1993 [Nucl. Phys. **A566**, 269c (1994)].
[20] R. Mattiello *et al.*, Phys. Rev. Lett. **63**, 1459 (1989).
[21] Y. Pang *et al.*, Phys. Rev. Lett. **68**, 2743 (1992).
[22] J. V. Allaby *et al.*, CERN Report No. 70-12, 1970 (unpublished); U. Becker *et al.*, Phys. Rev. Lett. **37**, 1731 (1976).
[23] NA35 Collaboration, R. Seyboth *et al.*, *QM'91 Proceedings*, Gatlinburg, 1991 [Nucl. Phys. **A544**, 293c (1992)].
[24] E. W. Beier *et al.*, Phys. Rev. Lett. **37**, 1114 (1976); V. Blobel *et al.*, Nucl. Phys. **B69**, 459 (1974); K. Guettler *et al.*, *ibid.* **B116**, 77 (1976).
[25] E-802 Collaboration, T. Abbott *et al.*, Phys. Rev. Lett. **66**, 1567 (1991).
[26] E-810 Collaboration, S. E. Eiseman *et al.*, Phys. Lett. B **292**, 10 (1992).
[27] E-810 Collaboration, K. J. Foley, *QM'91 Proceedings*, Gatlinburg, 1991 [Nucl. Phys. **A544**, 335c (1992)].
[28] E-814 Collaboration, J. Barrette *et al.*, Z. Phys. C. **59**, 211 (1993).
[29] E-814 Collaboration, P. Braun-Munzinger, *QM'91 Proceedings*, Gatlinburg, 1991 [Nucl. Phys. **A544**, 137c (1992)].
[30] E-814 Collaboration, J. Barrette *et al.*, Phys. Rev. C **46**, 312 (1992).
[31] S. Chapman and M. Guylassy, Phys. Rev. Lett. **67**, 1210 (1991); Phys. Rev. C **45**, 2952 (1992).
[32] G. E. Brown *et al.*, Phys. Lett. B **253**, 19 (1991).

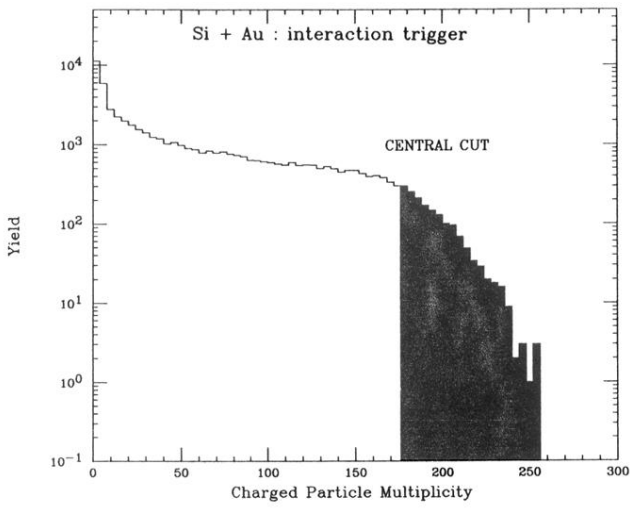

FIG. 3. Charged multiplicity for minimum bias collisions in the Si+Au reaction. The threshold corresponding to 7% of the interaction cross section is shown. Target-out contributions have not been subtracted.

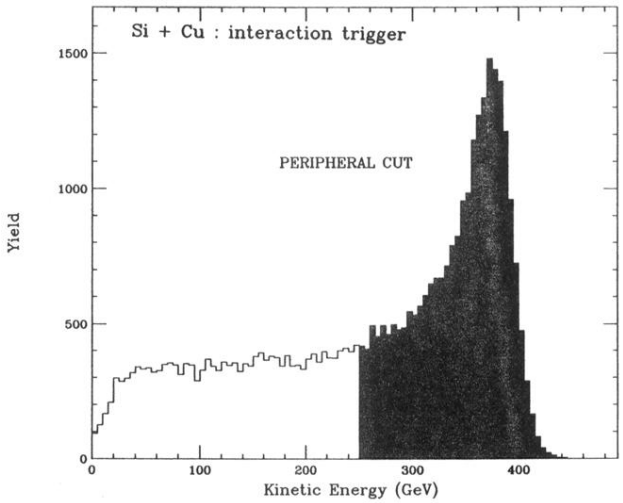

FIG. 4. Kinetic energy spectra of the projectile spectators in the Si+Cu reaction. The threshold corresponding to roughly 50% on the interaction cross section is shown. Target-out contributions have not been subtracted.